Synthesis of Nano-Silver Colloids and Their Anti-Microbial Effects

Guangyin Lei

Thesis submitted to the faculty of the Virginia Polytechnic Institute and State University in partial fulfillment of the requirements for the degree of

Master of Science
In
Materials Science & Engineering

Dr. Guo-Quan Lu, Chair
Dr. Kathleen Meehan, Co-Chair
Dr. Zhaomin Yang

November 8, 2007
Blacksburg, Virginia

Keywords: Silver nanoparticles; Bactericide; Escherichia coli; Staphylococcus aureus.

Synthesis of Nano-Silver Colloids and Their Anti-Microbial Effects

Guangyin Lei

Committee Chair: Dr. Guo-Quan Lu
Committee Co-Chair: Dr. Kathleen Meehan
Department of Materials Science & Engineering

ABSTRACT

The antimicrobial effects of silver nanoparticles were studied. Silver nanoparticles were synthesized through wet chemistry method, and were dispersed in an aqueous suspension. With nanoscale silica particles serving as heterogeneous nucleation sites, silver nanoparticles were formed on the silica surface. Suspensions were found to be stable at high silver concentrations as well as over a broad pH range. By varying the processing conditions, the diameter of the silver nanoparticles could be controlled between ~2 nm to ~25 nm. Scanning electron microscopy (SEM) and transmission electron microscopy (TEM) were used to reveal the formation and the corresponding morphology of the silver-silica coupling nanoparticles. Ultra-violet visible (UV-vis) scanning spectrophotoscopy was used to detect the distinct absorption spectrum of silver nanoparticles. The antimicrobial activities of these silver-silica coupling nanoparticles were investigated. *E. coli* and *S aureus* were used as representatives of Gram-negative and Gram-positive bacteria, respectively. Bacteriological tests showed either bacterial growth inhibition or cell death occurred, depending on the concentration of silver nanoparticles and the type of bacteria. Fluorescent microscopic images were also obtained to confirm the bacterial toxicity after exposure for several hours to silver nanoparticles.

ACKNOWLEDGEMENTS

I would like to express my deep gratitude and thankfulness to my advisor and committee chair, Dr. Guo-Quan Lu for his guidance and support throughout my Master's program of study. No matter what kind of problem was discussed, his advice and encouragement always provided new perspectives. The expertise that he shared with me remains a tremendous source for the professional growth to me. I am very thankful for everything he has done for me. Also I would like to voice my appreciation of Dr. Zhaomin Yang and Dr. Kathleen Meehan for serving on my committee, giving technical suggestions, and generously providing me the use of many lab facilities.

A special thank goes to Dr. Jesus N. Calata for his friendship, encouragement, suggestions, motivations, daily input, and the sharing of his expertise. All of his extraordinary help are greatly appreciated.

Other people from whom I benefited in this research including, within and outside of the group: Dr. Yang Xu, Dr. John G. Bai, Dr. Zach Z. Zhang, and Mr. Qian Xu. I have enjoyed doing research and discussing experimental details with them. Without their help, many things could have been much more difficult to achieve. I am also grateful to Stephen McCartney for his help with transmission electron microscopy, as well as scanning electron microscopy. His patience in helping me operate the equipment is greatly appreciated.

I owe my sincere appreciation to my family and relatives who have supported and encouraged me over the years. I would like to thank my beloved parents for their love, affection, and invaluable support.

Table of Contents

List of Figures

List of Tables

CHAPTER 1.
Introduction

Nanostructured materials have been the focus of intense research in recent decades due to their unique size-dependent physical and chemical properties[1-4]. Since the particle size can be tailored readily from 1 nm to 100 nm in diameter with moderate to excellent control over size uniformity, the resulting novel properties of these materials have been exploited for various optical and electrical applications, including nano-electronics, photonic crystals [5], and sensors based on surface enhanced Raman scattering [6 - 8] and near-field microscopy[9]. In addition, since a big proportion of biological problems deals with dimensions of micron and sub-micron, nanostructured materials can easily fit into these areas, and consequently play important roles. Topics in molecular recognition, biomolecule-nanocrystal conjugates as fluorescence label for biological cells, and DNA-mediated groupings of nanocrystals are widespread, intriguing people from both biological and engineering background. However, little yet is known about the biological systems response to the existence of these nanostructured materials. Some recent publications in the literature reported encouraging results of bactericidal properties of nanostructured materials. Hamouda *et. al.* [10] found a broad-spectrum sporicidal activity of certain nanoemulsions, which were stable, easily dispersed, nonirritant, and nontoxic in comparison with conventional agents. Klabunde *et. al.*[11] reported that nanosized magnesium oxide (MgO), adsorbed with halogen (Cl_2, Br_2), was effective against Gram-positive and Gram-negative bacterial cells as well as spores. In this study, the antimicrobial properties of silver nanoparticles are of specific interest.

Silver has been known to be a disinfectant for several centuries and has been widely used in the treatment of clinical diseases, including newborn eye prophylaxis and topical burn wounds[12-14]. Silver serves as a potent antibacterial

agent, acting against an exceptionally broad spectrum of bacteria while exhibiting low toxicity to mammalian cells. Since silver therapy is of significant clinical benefit in the control of bacterial infections, various forms of new agents medical, biological and pharmaceutical preparations [15-18] containing the silver ions, such as creams, solutions, electrodes, ligatures, biological skin and catheters, have been developed over the past decades. Therefore, not surprisingly, the antimicrobial properties of the silver ions have been extensively investigated[19,20], and many of the findings are well accepted universally.

However, research on the antibacterial effects of silver nanoparticles, another form of elemental silver, is still in its infant stage. Recently, Sondi *et al.*[21] reported the antibacterial properties of silver nanoparticles against a Gram-negative bacterium, *E. coli*; it was, to our knowledge, the first published article on the study of antibacterial properties of nanostructured silver. However, their experiments were complicated by the instability of their nanoscale silver suspensions. In this regard, this project is dedicated to carry out a technique to make stable aqueous suspension with high concentration of silver nanoparticles. Extensive bactericidal tests against both Gram-negative and Gram-positive bacteria were performed during the investigations of the antibacterial properties of silver nanoparticles.

Limited by the ultra high surface energy, and the correspondingly high particle activities, traditional methods of synthesizing the metallic nanoparticles, either physical methods or chemical methods, suffering from the poor particle stability and thus, cannot yield high nanoparticle concentrations in colloidal form. Therefore, regardless of surface chemistry of the metallic nanoparticles, organic or inorganic stabilizers are broadly applied to play the role of either physical or chemical barriers to preventing the particles from coalescencing or aggregating. In this study, as we aim at investigating the antibacterial properties of silver nanoparticles, the nanoparticles are required to have direct contact with the bacterial cells. Employment of an organic stabilizers or inorganic coatings would prevent thus contact, and is not preferred.

As a consequence, the first goal of the present study is to synthesis and stabilizes the silver nanoparticles using an alternative strategy. Nanoscale silica colloids, which possess extraordinary stability in high particle concentration and broad suspension pH, are employed as carriers of silver nanoparticles. Whereas silver and silica are metallic and insulating materials respectively, series of surface treatment of the silica nanoparticles have been applied to bond the silver nanoparticles. This strategy outweighs the other synthesizing methods in exposing the silver nanoparticles to surrounding medium. Furthermore, the suspension possesses excellent colloidal stability. Since no organic molecule is applied in the synthesis of nanoscale silver-silica composites, and because silica nanoparticles are supposed to be biocompatible to the bacterium, which was also confirmed through our tests, the antibacterial properties of silver nanoparticles can be easily identified.

The second goal of this project is to investigate the antibacterial properties of these nanoscale silver-silica composites. Since the antibacterial effects always fall into two categories, bactericidal and bacterial growth inhibitory, bacterial growth tests, bacterial viability tests are conducted from the different points of view, to further identify the antibacterial effects of these silver-silica composites.

A literature review of metallic nanoparticles is represented in the following chapter. Important aspects of metallic nanoparticles will be reviewed, including the traditional synthesis methods, their distinct chemical and physical properties, and some of their biological applications. Some basic concepts such as electric double layer, zeta potential, surface plasmon resonance, and bio-tagging will also be introduced.

Chapter 3 focuses on the experimental procedure. Detailed procedures on the synthesis of the nanoscale silver-silica composites, bacterial medium growth tests, and bacterial viability tests will be introduced, as well as some characterization approaches.

Chapter 4 is devoted to the results upon the experiments carried out in chapter 3. UV-vis scanning absorption spectrum and transmission electron microscopic images will be provided for the characterization of as-synthesized silver-silica coupling nanoparticles. Extensive information, such as silver nanoparticle size distribution, full width at half maximum (FWHM) of surface plasmon peak in the UV-vis absorption spectrum, will also be characterized. In regard of the antibacterial tests, bacterial growth curves, colonies on agar plates, and fluorescence microscopic images will be presented, and will be analyzed carefully.

Chapter 5 provides a discussion of the experimental results. General concerns on synthesizing silver nanoparticles, such as the selection of reducing agent and starting concentration of metallic ions will be included. The antibacterial effects of silver nanoparticles against *E. coli* and *S aureus* will be compared. However, since the physiological understanding of the differences is still lacking to date, we are not able to explain all the phenomena.

The last chapter, Chapter 6, summarizes the whole project, and makes a brief conclusion. Moreover, some of the future work will also be suggested in this chapter.

CHAPTER 2.
Literature Review

2.1. Synthesis of Metallic Nanoparticles

There are generally two approaches to synthesize nanostructure materials: top-down and bottom-up. Top-down methods reduce macroscopic particles to the nano scale size. Due to the lack of precise control over the experimental conditions, this route is usually not very well suited to the preparation of uniformly shaped particles; in addition, very small sizes are especially difficult to realize. On the contrary, bottom-up procedures are much better for generating uniform particles, of distinct size, shape, and structure. Bottom-up methods start with atoms that aggregate in solution or even in the gas phase to form particles of definite size, if appropriate experimental conditions are applied. However this bottom-up method always face the stability issue more than the top-down method because, in most of the cases, the particles are dispersed in aqueous suspension, the as-synthesized particles possess high mobility, and thus have better chance to collide with each other and form clusters or aggregations.

The synthesis of nanostructured materials from atomic or molecular sources depends on the control of a variety of nanoscale attributes desired in the final product. In general, the following four methods have been used to make nanostructured materials:

1. The first technique involves the production of isolated, ultrafine crystallites having uncontaminated free surfaces followed by a consolidation process either at room or at elevated temperature.

2. Chemical vapor deposition (CVD), physical vapor deposition (PVD), and some electrochemical methods have been used to deposit atoms or molecules of materials on suitable substrate.
3. By introducing defects in a formerly perfect crystal such as dislocations or grain boundaries, new classes of nanostructured materials can be synthesized. Subjecting the materials to high energy by either ball milling extrusion, shear, or high-energy irradiation may bring about such deformations.
4. The final approach used to make nanostructured materials is based on crystallization or precipitation from unstable states of condensed matter such as crystallization from glasses or precipitation from supersaturated solid or liquid solutions.

Although there are the general methodologies employed in the synthesis of nanostructured materials, several variants of these procedures have been developed to generate compounds or alloys with specific compositions and properties and also for optimized production.

There are basically two broad areas of synthetic techniques for nanostructured materials, namely, physical methods and chemical methods.

2.1.1. Physical Methods

Several different physical methods are currently in use for the synthesis of commercial production of nanostructures materials. The first technique, and the most widely used, involves the synthesis of single-phase metals and ceramic oxides by the inert-gas evaporation technique[22].

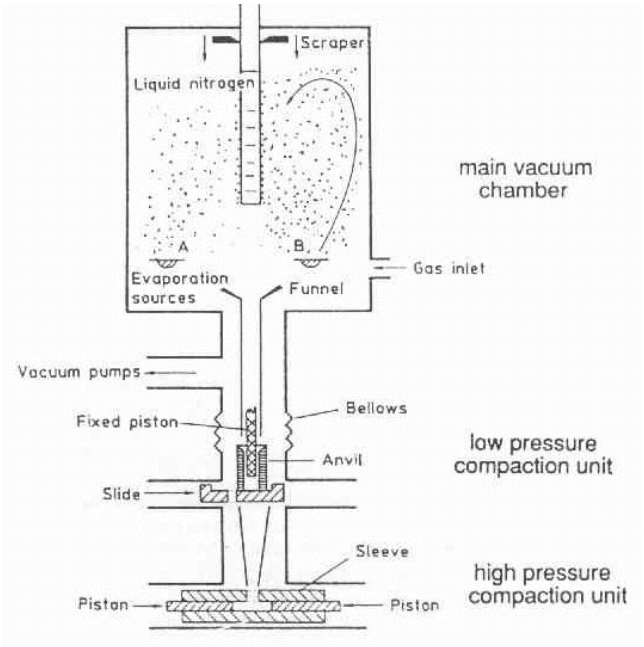

Figure 2.1: Apparatus for generating densely packed, monocomponent nanocrystalline material from gas aggregated clusters.

As depicted in Figure 2.1, the generation of atom clusters by gas phase condensation proceeds by evaporating a precursor material, either a single metal or a compound, in a gas maintained at a low pressure. The evaporated atoms or molecules undergo a homogeneous condensation to form atom clusters via collisions with gas atoms or molecules in the vicinity of a cold-powder collection surface. The clusters once formed must be removed from the region of deposition to prevent further aggregation and coalescence of the clusters. These clusters are then removed from the gas condensation chamber either by natural convection of the gas or by forced gas flow. The advantage of this method lies in the ease of control on the particle size by changing the removal speed, and as the particles are located specifically in the precursor sites, they are not tending to aggregate easily. However, contaminations can be introduced during the load and unload of the materials. This approach is preferable when large particle quantity is needed, and the particle size is not required to be highly uniform.

Sputtering is another technique used to produce nanostructured materials' clusters as well as a variety of thin films. This method involves the ejection of

atoms or clusters of designated materials by subjecting them to an accelerated and highly focused beam of inert gas such as argon or helium. The mechanism is somehow similar to the method above. The drawback is also the control of the uniformity of the particle size.

The third physical method involves generation of nanostructured materials via severe mechanical deformation. In this method, nanostructured materials are produced not by cluster assembly but rather by structural degradation of coarser-grained structures induced by the application of high mechanical energy. The nanometer-sized grains nucleate within the shear bands of the deformed materials converting a coarse-grained structure to an ultrafine powder. The heavy deformation of the coarse materials is affected by means of a high-energy ball mill or a high-energy shear process. Although this method is very useful in generating commercial quantities of the material, it suffers from the disadvantage that contamination problems result from the sources of the grinding media. The synthesized particles also tend to aggregate because they are directly contact each other without any effective separation mechanism. Another concern about this approach is that the particles cannot be made as really small size nanoparticles; the smallest size people get today is around 50 nm.

2.1.2. Chemical Methods

Chemistry has played a major role in developing new materials with novel and technologically important properties. The advantage of chemical synthesis is its versatility in designing and synthesizing new materials that can be refined into the final product. The primary advantage that chemical processes offer over other methods lies in good chemical homogeneity, as chemical synthesis offers mixing at the molecular level. Molecular chemistry can be designed to prepare new materials by understanding how material is assembled on an atomic and molecular level and the consequent effects on the desired material macroscopic properties. Basic understanding of the principles of crystal chemistry,

thermodynamics, phase equilibrium, and reaction kinetics is important to take advantage of the many benefits that chemical processing has to offer.

Solution chemistry (wet chemistry) is used sometimes to prepare the precursor, which is subsequently converted to the nanophase particles by nonliquid phase chemical reactions. Precipitation of solid from solution is a common technique for the synthesis of fine particles. The general procedure involves reactions in aqueous or nonaqueous solutions containing the soluble or suspended salts. Once the solution becomes supersaturated with the product, the precipitate is formed by either homogeneous or heterogeneous nucleation. After the nuclei are formed, their growth usually proceeds by diffusion. The growth rate of the nuclei after formation is very important in determining the formation of monodispersed particles. For instance, to prepare unagglomerated particles with a very narrow size distribution, all the nuclei must form at nearly the same time and subsequent growth must occur without further nucleation or agglomeration of the particles. In this regard, the selection of various chemicals, the determination of solution pH and chemical concentration as well as the reaction temperature are of extremely important to obtain fine particles.

In general, the particle size distribution, the physical properties such as crystallinity and crystal structure, and the degree of dispersion can be affected by reaction kinetics. In addition, the concentration of reactants, the reaction temperature, the pH, and the order of addition of reactants to the solution are also important. Even though a multielement material is often made by coprecipitation of batched ions, it is not always easy to coprecipitate all the desired ions simultaneously because different species may only precipitate at different pH. Thus, control of chemical homogeneity and stoichiometry requires a very careful control of reaction conditions.

However, there are certain difficulties in chemical processing. In some preparations, the chemicals are complex and hazardous. Contamination can also result from generation of the byproducts or side reactions in the chemical

process. This should be minimized or avoided to obtain desirable properties in the final products. Agglomeration can also be a major cause of concern at any stage in the synthesis process and it can dramatically alter the properties of the materials. As an example, agglomeration frequently makes it more difficult to consolidate nanoparticles to a fully dense compact. Finally, although many chemical processes are scalable for economical production, it is not always straightforward for all systems.

2.1.3. Stabilization of Nanoparticles against Agglomeration

Fine particles, particularly nanoscale particles, since they have large surface areas, often agglomerate to form either clusters or larger particles to minimize the total surface or interfacial energy of the system[23, 24]. When the particles are strongly stuck together, these hard agglomerates are called aggregates. Agglomeration of fine particles can occur at the synthesis stage, during drying and subsequent processing of the particles. Thus, it is very important to stabilize the particles against agglomeration at each step of particle production and powder processing.

Agglomeration of fine particles is caused by the attractive van der Waals force and/or the driving force that tends to minimize the total surface energy of the system [25]. Repulsive interparticle forces are required to prevent the agglomeration of these particles. Two methods are commonly used, namely, electrostatic and steric stabilization[26-28].

Electrostatic Stabilization

This method provides the dispersion by electrostatic repulsion. Most substances acquire surface electrical charges when brought in contact with a polar medium, resulting from one or more of the followings:

1. Preferential dissolution and salvation of surface species followed by dissociation of some of these species.

2. Lattice imperfection on solid surfaces.
3. Adsorption of ions or impurities at the solid-liquid interface.

As the surface electrical charges are formed, an unequal charge distribution always exists between a particle surface and the solvent, which depicted in Figure 2.2.

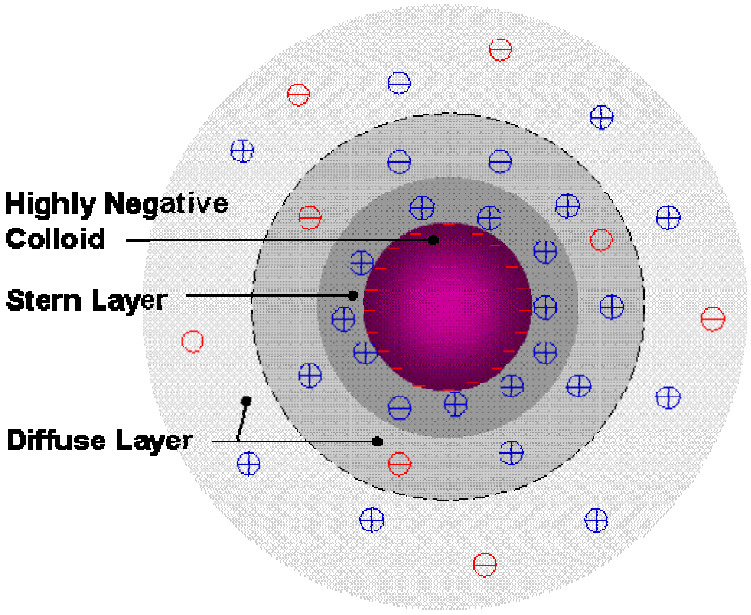

Figure 2.2: Distribution of electrical potential in the double layer region surrounding a charged particle showing the effective position of zeta potential.

The surface charge influences the spatial distribution of ions or molecules in the surrounding solution, attracting ions of opposite charge but repelling ions of similar charge from the surface. Along with the thermal motion, this leads to the formation of the diffused electrical double layer, which consists of the charged surface, neutralizing counter-ions, and, farther from the surface, co-ions distributed in a diffused manner[29,30]. The layer of counter-ions is known as Stern layer[31], and the diffuse layer can be visualized as a charged atmosphere surrounding the colloid. The charge density at any distance from the surface is equal to the difference in concentration of positive and negative ions at that point. Charge density is greatest near the colloid and gradually diminished toward zero as the concentration of positive and negative ions equal each other. The

thickness of this double layer depends upon the type and concentration of ions in solution.

The magnitude of the surface potential is related to the surface charge and the thickness of the double layer. As we leave the surface, the potential drops off roughly linearly in the Stern layer and then exponentially through the diffuse layer, approaching zero at the imaginary boundary of the double layer, as depicted in Figure 2.3. The potential measured at the interface of Stern layer and the diffuse layer is defined as zeta potential. The potential curve is useful because it indicates the strength of the electrical force between particles and the distance at which this force comes into play.

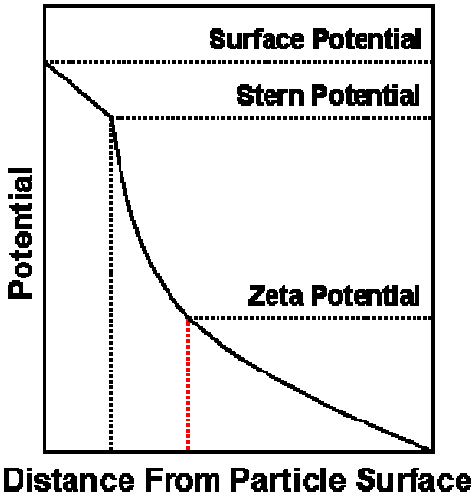

Figure 2.3: The numerical relationship between zeta potential and surface potential depends on the level of ions in the solution, as well as the ionic-ability of the solutes.

A charged particle will move with a fixed velocity in a voltage field. This phenomenon is called electrophoresis. The particle's mobility is related to the dielectric constant and viscosity of the suspending liquid and to the electrical potential at the boundary between the moving particle and the liquid. This boundary is called the slip plane and is usually defined as the point where the Stern layer and the diffuse layer meet. The Stern layer is considered to be rigidly

attached to the colloid, while the diffuse layer is not. As a result, the electrical potential at this junction is related to the mobility of the particle and is called the zeta potential. Although zeta potential is an intermediate value, it is sometimes considered to be more significant than surface potential as far as electrostatic repulsion is concerned.

Therefore, electrostatic stabilization of dispersion occurs when the electrostatic repulsive force overcomes the attractive van der Waals forces between the particles. The stabilization method is very sensitive to the electrolyte concentration since a change in the concentration may destroy the electric double layer, which results in particle agglomeration.

Steric Stabilization

The second method of stabilization involves the steric forces. Surfactant molecules can adsorb onto the surfaces of particles and their lyophilic chains will then extend into the solvent and interact with each other. The solvent-chain interaction, which is a mixing effect, increases the free energy of the system and produces an energy barrier to the closer approach of particles. When the particles come into closer contact with each other, the motion of the chains extending into the solvent become restricted and produce an entropic effect. Steric stabilization can occur in the absence of the electric barriers, and is effective in both aqueous and nonaqueous media. It is less sensitive to impurities or trace additives than electric stabilization. The steric stabilization method is particularly effective in dispersing high concentrations of particles.

Another steric stabilization takes advantages of core-shell geometry; the stability of the colloid will be greatly determined by the nature of the shell material. Silica shell is broadly applied for this purpose. It has been observed that silica nanoparticles in the size range of 10-100 nm possess a remarkable stability at very high salt concentration at pH >10.5, and even at their isoelectric point.

Comparing with the coating of a semiconductor with silica shell or coating a metallic nanoparticle with metal shell, coating of metallic nanoparticles with silica shell presents an additional difficulty, the lack of chemical affinity between the core and the shell materials. A procedure must be designed to overcome the very low tendency of the core and the shell materials to bond to each other. Several routes have been followed with better or worse results. Patil, Andres, and Otsuka [32] synthesized Au@SiO2 and Ag@SiO2 particles using a gas aggregation source. Though the technique can be employed to synthesize a whole range of particles, it suffers from many important disadvantages.

A much simpler procedure was used by Liz-Marzan and Philipse[33] for the synthesis of Au@SiO2 particles. The procedure was based on the formation of nanosized gold particles in the presence of small silica spheres, which led to heterocoagulation. The composite particles were then diluted with ethanol, where extensive growth was achieved by means of the Stober method[34], so that Au was embedded as a core. This synthetic route resulted in a mixture of unlabeled and labeled silica particles, with a low proportion of the coated particles.

Another method that has provided substantially better results was later designed by Liz-Martan, Giersig, and Mulvaney[35-37]. The method was based on the use of silane coupling agents as surface primers to provide the nanoparticle surface with silanol groups, and therefore to render the surface of noble metals compatible with silicate moieties. Once the surface had been modified, slow deposition of a thin silica shell was effected from a solution of active silica. Subsequent transfer into ethanol led to sudden condensation of unreacted silicate, which can yield nicely concentric Au@SiO2 core shells. The shells could then be grown by careful addition of ammonia and tetraethoxysilane, resulting in monodisperse colloids as shown in Figure 2.4.

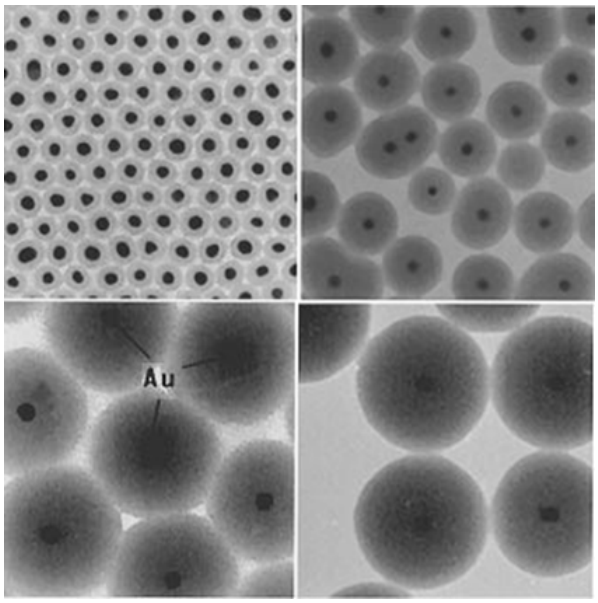

Figure 2.4: Uniform core-shell particles obtained by controlled dilution with ethanol and successive growth by TES hydrolysis[37].

The interest in core-shell nanoparticles, is not just due to the enhancement of colloidal stability, but has been driven by the interest in creating nanomaterials and nanostructures with unique, complex properties. The properties of interest are mainly optical, electronic, and magnetic[38-40].

2.2. Optical Properties of Metallic Nanoparticles

Probably the optical property of nanoscale metallic particles is one of the most interesting topics in nano-related researches. Colloidal metallic nanoparticles possess optical absorption spectra with an absorption peak that looks similar to the absorption peak of colloidal semiconductor quantum dots. However, this absorption does not derive from transitions between quantized energy states. Instead, in metallic nanoparticles, collective modes of motion of the electron gas can be excited. They are referred to as localized surface plasmons. The peak in the absorption spectrum is the resonance frequency for the generation of surface plasmons. Therefore, the size dependence is not that significant comparing with semiconductor quantum dots.

The purpose of this section is to give an overall review on basic concepts in the optical properties of metallic nanoparticles, especially on noble metals, like gold and silver. Origin of the surface plasmons, size/shape related phenomenon, and dispersion medium influences will be discussed in detail.

2.2.1. Surface Plasmons in Spherical Metallic Nanoparticles

The strong optical extinctions of conductive metal nanoparticles arise from an electrodynamic phenomenon known as surface plasmons, which are generated by the collective excitation of free electrons in response to a characteristic electromagnetic frequency.

Surface plasmons can be categorized into two types: localized plasmon resonance, in which incident light is absorbed or scattered by the oscillating electric dipoles within a metal nanoparticle, and surface plasmon polaritons, which propagate along metal surfaces in a waveguide-like fashion until released at some distance from their point of origin. These two types are depicted in Figure 2.5. Localized plasmon resonance is important for generating local field factors, which enhance linear and nonlinear optical effects near the metal surface. However, metal nanostructures often support both types of plasmons simultaneously, surface plasmon resonance (SPR) and surface-enhanced Raman scattering (SERS)[41-43] and it is difficult to decouple one from the other.

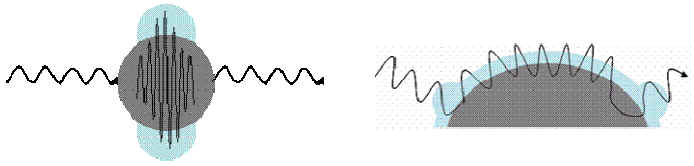

Figure 2.5: Incident light on nanostructured metal surfaces can generate localized (standing) plasmon resonances (left) as well as surface waves (right). Excitation of conduction electrons produces local electromagnetic fields near the metal surface.

In the simplified case of a metal nanosphere with radius R much smaller than the incident wavelength (a condition commonly referred to as the quasi-static approximation), the plasmon response is essentially dipolar in nature. The strength and frequency of this resonance is related to the total number of electrons in the oscillating dipole (defined essentially by the particle volume, or R^3), the complex dielectric function $\varepsilon(\omega)$, and the dielectric constant of the local medium ε_d. The plasmonic response is directly measurable by optical extinction and can be quite intense.

Extinction includes both absorption and scattering components, which have different scaling relationships with nanoparticle size. The absorption cross section increases linearly with particle volume, whereas the scattering cross section is relatively smaller but scales with volume squared. Such power functions are approximate and deviate significantly for particles above the quasi-static size limit. The dipolar plasmon response (oscillator strength) of the nanoparticle is often defined by its polarizability, which can be expressed by the electrostatic Lorentz-Lorenz equation:

$$a = 4\pi\varepsilon_0 R^3 \left| \frac{\varepsilon - \varepsilon_d}{\varepsilon + 2\varepsilon_d} \right| \tag{2.1}$$

The resonance condition leading to maximum polarization is $\left|\varepsilon + 2\varepsilon_d\right| = 0$, requiring $\varepsilon(\omega)$ being negative. However, the complex dielectric function should be divided into real and imaginary components $\varepsilon'(\omega)$ and $\varepsilon''(\omega)$ in order to remove the phase-dependent term from the equation; resonance is thus achieved when $\varepsilon'(\omega) = -2\varepsilon_d$ and $\varepsilon''(\omega) << 1$. The dielectric function is negative when ω is below some threshold frequency ω_p, known also as the plasma frequency. The relationship between $\varepsilon(\omega)$ and ω_p can be illustrated by the Drude model, a conceptually useful description of free-electron behavior in metals.

Here $\varepsilon'(\omega)$ and $\varepsilon''(\omega)$ can be approximated in terms of ω_p and Γ, the plasmon relaxation frequency:

$$\varepsilon'(\omega) \approx 1 - \frac{\omega_p^2}{\omega^2 + \Gamma^2} \tag{2.1}$$

$$\varepsilon''(\omega) \approx \frac{\omega_p^2 \Gamma}{\omega(\omega^2 + \Gamma^2)} \tag{2.3}$$

Applying these relations to Eq. (2.1) yields a Drude resonance frequency $\omega_D = \omega_p / \sqrt{2\varepsilon_d + 1}$ when $\varepsilon''(\omega)$ is small. The plasma frequency ω_p is a bulk material property and is scale-invariant within the quasi-static limits. However, the Drude free-electron response varies with geometric shape, which suggests a useful theoretical handle for predicting characteristic resonance frequencies of ellipsoids and other anisotropic particles as a function of aspect ratio.

However, the free electron cannot be directly applied in calculating the plasmonic response of most metals of interest because of the additional electric susceptibility introduced by interband transitions between the outermost d and s orbital at optical frequencies (threshold excitation energies for Ag ($4d \rightarrow 5s$) and Au ($5d \rightarrow 6s$) are close to 3.9 and 1.8 eV, respectively). These electronic excitations will change $\varepsilon'(\omega)$ and $\varepsilon''(\omega)$; in addition, they can provide a significant relaxation (damping) mechanism for plasmon decay, reducing the quality of the optical resonance. In the case of Ag, interband transitions are responsible for changes in the resonance condition and the subsequent frequency difference between the theoretical Drude response ($\omega_D = 5.6eV$) and the observed plasmon resonance ($\omega_{sp} = 3.6eV$). In the case of other metals such as Au and Cu, $\varepsilon''(\omega)$ cannot be neglected at optical frequencies so the resonance condition derived from Eq. (2.1) is no longer strictly applicable.

Exact solutions for the optical properties of metal nanostructures can be obtained instead using electrodynamic Mie theory, whose formulations are derived from Maxwell's equations. Applications of Mie theory requires the input of ε_d and $\varepsilon(\omega)$ as a function of frequency for a given particle size, either as experimental values or as numerical approximations. Various optical functions can be calculated with great accuracy; for example, extinction and optical conductivity (ε''/λ) spectra of Cu, Ag, and Au particles in the quasi-static limit were calculated using Eq. (2.4), with the effect of ε'' on the resonance band plainly visible. The calculated extinctions reproduce the experimental spectra with a high degree of fidelity with the exception that it does not include scattering.

$$\sigma_{ext}(\omega) = \frac{12\pi\varepsilon_d^{3/2}R^3\omega}{c}\left|\frac{\varepsilon''}{(\varepsilon'+2\varepsilon_d)^2+(\varepsilon'')^2}\right| \tag{2.4}$$

Mie theory has been used to estimate variations in the electrodynamic response due to particle size, anisotropy, and other extrinsic parameters. This includes metallic nanoparticles beyond the quasi-static limit ($2R/\lambda > 0.05$), whose plasmon resonances are red shifted by phase retardation and broadened by radiation damping. Higher-order plasmon modes also become significant; for example, quadrupole resonances in Ag and Au particles can be observed in optical extinction spectra starting from ~60 nm.

Another important transition takes place in the mid-nanometer size regime: scattering supersedes absorption as the dominant optical response, at about 60 nm for Ag and 80 nm for Au. Dipole (S_1) scattering typically provides the largest contribution, followed by quadrupole (S_2) scattering. As particles continue to increase in size, the various absorption and scattering modes reach a maximum, and then fade away until only the bulk optical properties of the metal remain.

2.2.2. Surface Plasmons and the Metal Function

Besides the interband transition, which has great impact on the free-electron plasmon response, several other material factors also have an influential role on surface plasmons and $\varepsilon(\omega)$: (a) the electron mean free path, (b) the skin depth, and (c) local medium effects.

Size confinement effects on the plasmon band

Metallic nanoparticles exhibit peak broadening when their diameters are much less than the electron mean free path L_e, a material-dependent property describing the quasi-elastic scattering of conduction electrons (L_e in bulk Ag and Au are about 50 nm and 40 nm, respectively). The effective path length L_r decreases almost linearly with $2R$, corresponding with a change in $\varepsilon(\omega)$ from the bulk dielectric function. Broadening of the plasmon band in Ag and Au nanoparticles becomes evident for $2R < 10$ nm; the plasmon resonance frequency is not affected, but the relaxation rate Γ increases with a $1/R$ relationship due to the greater electron scattering by the particle surface. In the case of the very smallest nanoclusters ($2R < 2$ nm), the local density of states may be reduced to the extent that they no longer form a continuous band structure.

Skin depth

The incident light on a bulk metal surface has a low penetration depth, with an exponential attenuation of electric field strength below the surface. The electric field within the metal can be expressed as a function of depth z:

$$\left|E(z)\right| = \left|E_0\right| e^{-z/\delta} \tag{2.5}$$

Here the skin depth δ is defined as

$$\delta = \frac{c}{\omega k} = \frac{\lambda}{2\pi k} \tag{2.6}$$

where k is the absorption coefficient of the metal. The bulk refractive index n and the absorption coefficient k are related to the complex dielectric function by $n+ik=\sqrt{\varepsilon'+\varepsilon''}$, so k can be expressed in terms of the dielectric function as

$$k=\sqrt{\frac{(\varepsilon')^2+(\varepsilon'')^2-\varepsilon'}{2}} \tag{2.7}$$

Calculations of δ using Eq. (2.6) and (2.7) at different optical wavelengths suggest an average value of ~30 nm for both Ag and Au. This reaffirms the dipolar nature of localized plasmon resonances for nanoparticles with diameters on the order of L_e, and suggests the onset of multimode plasmon modes in larger metal nanoparticles.

Local dielectric and surface effects

Coupling between the Drude free-electron response and interband excitations can be weakened by modulating ε_d, such that the Drude frequency is shifted away from the electronic transition threshold. An especially dramatic effect can be expected in the case of Cu, which has a significant $\varepsilon''(\omega)$ at plasmon frequencies above $2\,eV$. By embedding Cu nanoparticles in transparent media with ε_d>5, the plasmon resonance frequency of Cu nanoparticles can be lowered to below $2\,eV$, resulting in a large enhancement in optical extinction.

Metal nanoparticles are also solvatochromic; polymer-stabilized Au particles dispersed in organic solvents of varying refractive indices (n=1.33-1.60) demonstrated a shift in absorption from red to purple, accompanied by an increase in extinction intensity. The experimental data was found to be in excellent agreement with Mie theory, based on the changes in ε_d.

Surface adsorbates (ligands) can also influence the optical properties of metal nanoparticles. Strongly adsorbing anions and chemisorptive surfactants such as thiols accelerate plasmon relaxation, resulting in peak broadening. This

effect has been attributed to a reduction in conduction electron mobility, due to electronic coupling between the plasmon and charge-transfer bands formed by the metal-adsorbate complex. Strong optical resonance can be restored in some cases by cathodic (negative) charging, which induces ligand desorption.

Plasmon decay and radiative damping

The quality of the dipolar plasmon response depends both on the intensity of polarizability and the coherence lifetime of the collective oscillations. The latter is determined by the dephasing (or decay) of the collective dipole. Plasmon relaxation occurs by radiative damping and also by nonradiative electronic mechanisms such as interband transitions. Radiative damping of an oscillating electronic dipole is the electromagnetic equivalent of mechanical damping in a vibrating system, with the conduction electrons providing an effective mass.

Both radiative damping and polarizability increase with particle volume, such that the increased dipole oscillator strength is accompanied by broadening of the optical response. Radiative damping also scales with $1/\lambda^3$, with a consequently reduced effect on plasmons at lower frequencies. Radiative damping in single metal nanoparticles has recently been measured using near-field scanning optical microscopy, which permitted quantitative determination of plasmon linewidths (Γ) from individual nanoparticles. These were narrower than that produced by bulk measurements, and yielded an excellent correlation between experiment and Mie theory.

As a practical rule, damping and phase-retardation effects in spherical nanoparticles will have a compromising effect on optical emission and field-enhanced applications such as SERS when $2R/\lambda > 1/\pi\sqrt{\varepsilon_d}$ (approximately 0.24 in water). However, it is important to mention that radiative damping is not necessarily dependent on the overall particle volume, but rather on those portions, which define an “optical domain.”

2.3. Biological Applications of Metallic Nanoparticles

Living organisms are built of cells that are typically around 10 um in size. However, the cell parts are much smaller and are in the sub-micron size domain. Even smaller are the proteins with a typical size of just 5 nm, which is comparable with the dimensions of smallest man-made nanoparticles. This simple size comparison suggests that nanoparticles may be used as very small probes that would allow us to detect at the cellular stage without introducing too much interference. Understanding of biological processes on the nanoscale level is a strong driving force behind development of nanotechnology.

This section will cover some of the fundamental ideas of biological applications of metallic nanoparticles, and gives an overview of current developments in anti-microbial research area.

2.3.1. General Applications in Biological Area

As mentioned above, the fact that nanoparticles exist in the same size domain as proteins makes nanoparticles suitable for bio-tagging or –labeling. Here is a list of some of the applications of nanoparticles in biological and medicine fields:

- Fluorescent biological labels[41,42];
- Drug and gene delivery[43,44];
- Bio detection of pathogens[45];
- Detection of proteins[46];
- Probing of DNA structure[47];
- Tissue engineering[48];
- Tumor destruction via heating[49];
- Separation and purification of biological molecules and cells[50];
- MRI contrast enhancement[51].

However, size is just one of many characteristics of nanoparticles that itself is rarely sufficient if one is to use nanoparticles as biological tags. In order to interact with biological target, a biological or molecular coating or layer acting as a bioinorganic interface should be attached to the nanoparticles. Examples of biological coatings may include antibodies, biopolymers like collagen, or monolayers of small molecules that make the nanoparticles biocompatible. In addition, as optical detection techniques are wide spread in biological research, nanoparticles should be able to either couple with fluorescent materials or change their optical properties during the application.

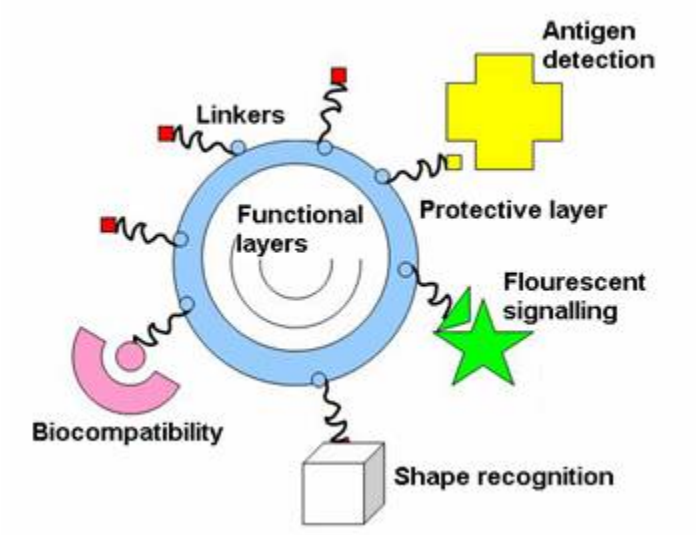

Figure 2.6: A general model of nanoparticles in biological applications. From the view point of multi-functional, several functional groups can be attached on the nanoparticle's surface, and thus enabling the nanoparticle in detecting, transporting, and even destroying the biological molecules, which are of interested.

As depicted in Figure 2.6, nanoparticle usually forms the core of the system; it can be used as a convenient surface for molecular assembly, and may be composed of inorganic or polymeric materials. It can also be in the form of nano-vehicle surrounded by a membrane or a layer. The size and size distribution might be important in some cases, for example if penetration through

a pore structure of a cellular membrane is required. The core itself might have several layers and be multifunctional. For example, by combining magnetic and luminescent layers, one can both detect and manipulate the particles. The core particle is often protected by several monolayers of inert material, such as silica. Organic molecules that are adsorbed or chemisorbed on the surface of the particle are also used for this purpose. The same layer might act as a biocompatible material. More often, an additional layer of linker molecules is required to proceed with further functionalization. The linear linker molecule has reactive groups at both ends. One group is aimed at attaching the linker to the nanoparticle surface and the other is used to bind various moieties like antibodies, fluorophores, etc., depending on the function required by the application.

2.3.2. Population Growth of Bacteria

Growth is an orderly increase in the quantity of cellular constituents. It depends upon the ability of the cell to form new protoplasm from nutrients available in the environment. In most bacteria, growth involves increase in cell mass and number of ribosomes, duplication of the bacterial chromosome, synthesis of new cell wall and plasma membrane, partitioning of the two chromosomes, septum formation, and cell division.

Under favorable conditions, a growing bacterial population doubles at regular intervals. Growth is by geometric progression: 1, 2, 4, 8, etc. or 2^0, 2^1, 2^2, 2^3… 2^n (where n is the number of generations). This is called exponential growth. In reality, exponential growth is only part of the bacterial life cycle, and not representative of the normal pattern of growth of bacteria in nature.

When a fresh medium is inoculated with a given number of cells, and the population growth is monitored over a period of time, plotting the data will yield a typical bacterial growth curve. The bacterial growth curve is naturally divided to four parts, as duplication rate is taken into consideration.

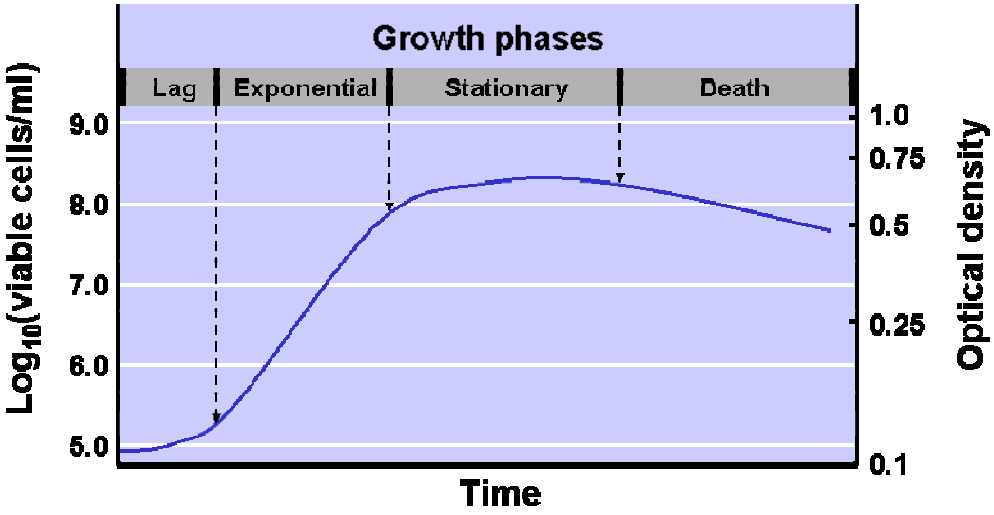

Figure 2.7: A typical bacterial growth curve. Four distinct phases can be recognized, which are lag phase, exponential phase, stationary phase, and death phase respectively. These phases are different from the viewpoint of contributing to bacterial duplication, and are mainly recognized by bacterial growth rate.

Four characteristic phases of the growth cycle are recognized:

1. **Lag Phase.** Immediately after inoculation of the cells into fresh medium, the population remains temporarily unchanged. Although there is no apparent cell division occurring, the cells may be growing in volume or mass, synthesizing enzymes, proteins, RNA, and increasing in metabolic activity. The length of the lag phase is apparently dependent on a wide variety of factors including the size of the inoculum; time necessary to recover from physical damage or shock in the transfer; time required for synthesis of essential coenzymes or division factors; and time for synthesis of new enzymes that are necessary to metabolize the substrates present in the medium.
2. **Exponential (log) Phase.** The exponential phase of growth is a pattern of balanced growth wherein all the cells are dividing regularly by binary fission, and are growing by geometric progression. The cells divide at a constant rate depending upon the composition of the growth medium and the conditions of incubation. The rate of exponential growth of a bacterial

culture is expressed as generation time, also the doubling time of the bacterial population. Generation time (G) is defined as the time (t) per generation (n = number of generations). Hence, G=t/n is the equation from which calculations of generation time (in the next section) derive.

3. **Stationary Phase.** Exponential growth cannot be continued forever in a batch culture (e.g. a closed system such as a test tube or flask). Population growth is limited by one of three factors: 1. exhaustion of available nutrients; 2. accumulation of inhibitory metabolites or end products; 3. exhaustion of space, in this case called a lack of "biological space". During the stationary phase, if viable cells are being counted, it cannot be determined whether some cells are dying and an equal number of cells are dividing, or the population of cells has simply stopped growing and dividing.
4. **Death Phase.** If incubation continues after the population reaches stationary phase, a death phase follows, in which the viable cell population declines. However, this decline cannot be observed by turbidimetric measurements. During the death phase, the number of viable cells decreases geometrically (exponentially), essentially the reverse of growth during the log phase.

Growth Rate and Generation Time

Bacterial growth rate and generation time are two of the most important aspects in regard of bacterial growth. The determination of bacterial growth rate will give us a general sense of how the bacterial cells response to its environment. As mentioned above, bacterial growth rate during the phase of exponential growth, under standard nutritional conditions (culture medium, temperature, pH), defines the bacterium's generation time. An alternative way of defining the bacterial generation time is that it is the time interval required for the cells (or population) to divide. Generation times for bacteria vary from about 12 minutes to 24 hours or more. Even for the same bacterium, the generation time may be quite different depend on the inoculation conditions, and on the initial

bacterial concentration. The generation time for *E. coli* in the laboratory is typically 15 to 20 minutes, and for *S. aureus* is around 27 to 35 minutes.

Calculation of Generation Time

When growing exponentially by binary fission, the increase in a bacterial population is by geometric fashion. If we start with one cell, when it divides, there are 2 cells in the first generation, 4 cells in the second generation, and 8 cells in the third generation, and so on. Therefore we can easily derive the equations for calculating the bacterial generation time, based on some simply mathematic transformations. The relation can be presented as follows:

$$G = \frac{t}{3.3\log(b/B)} \tag{2.8}$$

where G is the bacterial generation time; B is the number of bacteria at the beginning of a time interval; b is the number of bacteria at the end of a time interval; t is the time interval for hours or minute.

Hence, by comparing the typical bacterial generation time and the experimental data, it is not difficult to find out the bacteriological properties of nanoparticles added into the bacterial medium.

2.3.3. Bactericidal Effects of Metallic Nanoparticles

People have known about the bactericidal properties of many metallic ions, as well as bulk metals for a long time. Enormous work has been dedicated to find out the fundamental physical and biological mechanisms for these metallic ions, and some satisfactory explanations have been derived. However, knowledge nowadays in biological and anti-pathogen properties of

nanostructured materials is still limited, especial for the nanostructured metals in the anti-bacteria field.

Some of the recent studies reported encouraging results of bactericidal properties of several nanostructured materials. Hamouda *et al.*[10] revealed the broad-spectrum sporicidal activity of certain nanoemulsions. These nanoemulsions were also found to be stable, easily dispersed, nonirritant, and nontoxic compared with other agents. Klabunde *et al.*[11] reported that when significantly adsorbed with halogen (Cl_2, Br_2), magnesium oxide (MgO) was very effective against Gram-positive and Gram-negative bacterial cells as well as spores[52]. These studies only provided us a possible approach in bactericidal study using nanostructured materials.

To find a more direct fashion to discover the bactericidal properties of nanostructured materials, researchers turn their focus on some well known bactericidal metals. As is well known, some elements by themselves are harmful to microorganisms, and silver is the most toxic one among them[53,54]. Therefore, silver ions and silver-containing products are widely used in medical applications. For instances, silver compounds are used for treatment of serious burns, in bandages for trauma and diabetic wounds[55], and are used to coat the catheters and other medical devices to prevent the growth of bacterial biofilms[56]. Numerous studies have done to reveal the mechanisms of bactericidal property and even bacterial resistance of silver ions[19,20]. And in regard of nanostructured silver, not until recently, Sondi *et al.*[21] reported the antimicrobial property of silver nanoparticles against *E. coli*, which is a gram-negative bacterium[57]; it was the

first paper on the study of bactericidal property of nanostructured metal. Conclusively, the silver nanoparticles used in their experiment to some extent possessed bactericidal effects, as the biological tests in agar plates showed that only few bacterial colonies were formed under the treatment of silver nanoparticles. And in the medium culture tests, notable difference between control sample and the samples mixed with silver nanoparticles had been found. However, from the efficiency point of view, their experiments were limited due to the non-ideal stability of the silver nanoparticles. The silver-containing samples were found not stable after the mixing of silver nanoparticles and bacterial culture.

The possible explanation is given to the surface charge attraction of bacterial cells and the silver nanoparticles. In addition, the dispersion of nanostructured materials, which is also called a colloid, is very sensitive to the liquid medium. Colloidal system stability can be easily destroyed by changing the medium pH or even environmental temperature. As a consequence, since there is no biological benign stabilizer in their test, the colloidal stability can not be sustained when mixed with bacterial medium. Silver nanoparticlessoon agglomerated together and eventually precipitated down to the bottom of the testing tubes, and resulted in the reduction of bactericidal effects.

CHAPTER 3.
Experimental Procedure

3.1. Synthesis of Silver Nanoparticles

Silver nanoparticles used in the experiments were synthesized through wet chemical method, and were dispersed in aqueous suspension. The solvent can actually be polar or non-polar, depending on specific requirements. From the stability point of view, silica nanoparticles, which were served as the carriers of silver nanoparticles, were employed as the stabilization agents. The synthesis procedure consisted of modifying the surface of the silica spheres with Sn^{2+} ions and then carrying out a redox reaction in which Sn^{2+} ions were oxidized to Sn^{4+} ions while Ag^{+} ions were reduced to metallic Ag^{0}, which stayed attached on the silica surface in the form of nucleus. Afterwards, addition of excess reducer would reduce more and more Ag^{+} ions to Ag^{0}. These "fresh" Ag^{0} atoms would attach on the existing Ag nucleus, and therefore undergoing a growth phase. Control of the silver nanoparticles size could be achieved by choosing the reducer and concentrations and even the speed of addition, as well as by adjusting the concentration of the silver ions. Although temperature also played an important role, we did not conduct our experiments such that we controlled the reaction temperature.

3.1.1. Chemicals

Silver nitrate ($AgNO_3$, ACS, 99.9% metal basis) and colloidal silica suspension (14-nm, 40-wt% in water) were supplied by Alfa Aesar. Sodium borohydride ($NaBH_4$) and tin (II) chloride ($SnCl_2$) were obtained from Sigma Aldrich. All chemicals were used as received. All glassware used in the

synthesis of silver nanoparticles were cleaned with aqua regia (3 parts HCl, 1 part HNO_3), rinsed with 18.3-MΩ nano-pure water, and oven dried prior to use.

3.1.2. Surface Activation of Silica Nanoparticles

The mean diameter of silica nanoparticles was 14 nm, and the suspension has a solid loading of 40 percent by weight of silica with excellent stability over a broad range of pH, from 6 to 12. As a matter of fact, a non-polymeric surfactant, sodium oxide (Na_2O), was already added by the manufacturer to keep the colloidal suspension stable. As introduced in the former section, based on the knowledge of particle surface charge and zeta-potential, and as the Na^+ ions were adsorbed on the surface of silica nanoparticles, this localized high ionic density would cause the re-distribution of molecular ions in suspension by electrostatic mean, therefore, greatly enhanced the colloids' zeta potential, and resulting in the high system stability.

Surface activation of silica nanoparticles started with the adsorption of Sn^{2+} ions. As there are naturally lots of hydroxyl groups adsorbed around the silica nanoparticles when in aqueous suspension, they turn to form the ion equilibrium with the Sn^{2+} ions surrounding the particles; the chemical equilibrium equation is presented as follows:

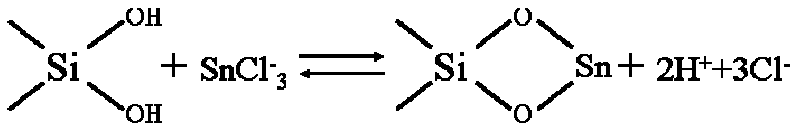

The ionic equilibrium could be easily controlled by adjusting the suspensions' pH, using low concentrations of HCl or NaOH. By doing this, we can control the direction of chemical reaction, and eventually determine the amount of Sn^{2+} ions adsorbed on silica nanoparticles. This process was actually the same as the pretreatment of non-metallic substrate for electroless plating. The successful adsorption of Sn^{2+} ions will result in good attachment of silver nanoparticles on these silica nanoparticles, and vica versa.

For the experimental construction, an aqueous solution of silica nanoparticles (2.4 wt%, 150 ml) was mixed with 15 ml of $SnCl_2$ solution (0.05M) rapidly under violent stirring for up to 30 minutes. Empirically, this time period should be enough for the adsorption of Sn^{2+} ions. In addition, since the solution's pH is also critical for the chemical equilibrium, we adjust the pH to around 6, which is a little bit acidic. The reason of doing this is that the acidic environment favors the chemical reaction to anchor more Sn^{2+} ions on the silica surface, and the pH will also maintain the stability of Sn^{2+} and prevent its oxidation to Sn^{4+}. Since our purpose was nucleating the silver nanoparticles on the surface of silica nanoparticles, the Sn^{2+} ions should be controlled to exist only on the silica surface. Therefore, the nanoparticles were centrifuged several times to get rid of the excess Sn^{2+} ions in suspension and then were resuspended in DI water. Centrifugation conditions in this experiment were very picky. Since the particles that we were using were extremely small, large relative centrifugal force (RCF) should be applied with long centrifuge time. Specifically, RCF of 20,000g and a time period of 2 hours were found to be effective. After each centrifugation, the supernatant was removed, and the precipitate down on the bottom of the centrifuge tube was re-dispersed in deioned water with the help of ultrasound. This washing process was repeated several times to insure removing the excess Sn^{2+} ions.

3.1.3. Heterogeneous Nucleation of Silver Nanoparticles

The heterogeneous nucleation of silver nanoparticles was then executed after the surface activation of silica nanoparticles. High purity silver nitrate ($AgNO_3$), dissolving in deioned water, was used for providing the Ag^+ ions (5 mM, 20 ml). Fresh prepared silver nitrate solution was quickly added into the aforementioned surface-activated silica suspension (100 ml), under the condition of violent stirring. Redox reaction was observed immediately after mixing, the mixture changed color from clear to pale yellow, which indicated the formation of small sized silver nanoparticles. The designed reaction was:

$$Sn^{2+} + 2Ag^{+} \longrightarrow Sn^{4+} + 2Ag^{0}$$

Since Sn^{2+} ions were only adsorbed on the surface of silica nanoparticles, the silver atoms formed should also be found homogeneous to grow silver nanoparticles in that region, and will later play the role of growth nucleus.

Later on, as more and more Ag atoms were reduced, these atoms would either follow the catalytical pathway or collision procedure, to form the stable nucleus on the surface of silica nanoparticles. To ensure the stability and uniformity of this nucleus, the mixture was stirred for up to one hour. At this stage, the ratio of Ag ions and the silica nanoparticles is crucial in determining many of the properties of silver nanoparticles, which will be formed later. This ratio, to some extent, directly determined the number of silver nanoparticles, and, in addition, will affect the size of as-formed silver nanoparticles. Another requirement for the success of the heterogeneous nucleation of silver atoms is that the DI water used in the experiment should be of high purity. The presence of other metallic ions or acid/basic groups will seriously affect the formation of on-silica silver nucleus. The impurities may change the redox reaction potential or contaminate the silica surface, with the result that free standing silver nucleus will be formed in the suspension.

3.1.4. Growth of Silver Nanoparticles

The third and the last phase for synthesis the silver nanoparticles was the growth of silver nanoparticles. Since the growth of nanoparticles required lots of metallic atoms, in this experiment, a chemical reducer was then employed after the formation of silver nucleus. Since the silica nanoparticles were only 14 nm in diameter, it was not practical to synthesis large silver nanoparticles on its' surface. As a consequence, to limit the particle size, a strong reducer, sodium borohydride ($NaBH_4$, 0.4M/L), was used to make small silver nanoparticles.

$$Ag^{+} + BH_4^{-} + H_2O \longrightarrow Ag^{0} + BH_3^{+} + OH^{-}$$

Herein, some criteria should be addressed. The concentration of the reducer and the relative concentration to silver ions should be determined according to different purpose. In general, a low reducer concentration would result in small number of silver nanoparticles, with large particle size; otherwise, high reducer concentration would bring to large number of silver nanoparticles, with relatively small particle size. Therefore, the total number of silver nanoparticles was actually determined by the combined effects of the first step, the tin-driven nucleation, and the strong reducer caused Oswald ripening later in the growth phase of silver nanoparticles. As long as the surface of silica nanoparticles was large enough, the as-formed silver nanoparticles were always small with narrow size distribution; otherwise, the newly formed silver nucleus would found not enough space to attach, and thus turned to form larger particles instead of stayed apart from each other.

In conclusion, the whole process of synthesizing silver nanoparticles would be depicted by Figure 3.1.

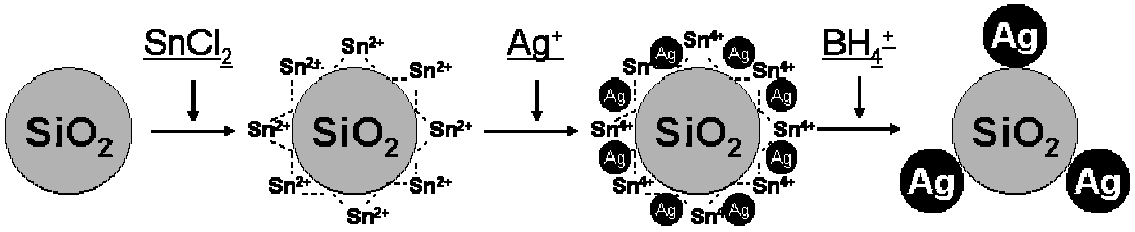

Figure 3.1: A schematic to show the mechanism of how the silver-silica nano-composites were synthesized. At the first stage, the surface of silica nanoparticles been activated by Sn^{2+} ions, and were them anchored with Ag^0 atoms. Afterwards, assisted by the reducing agent, more and more silver ions were reduced, and as a consequence attached on the existing silver atoms. Through an initial nucleation phase and carried out the Oswald ripening, small silver nucleus were then formed. At last, as still more silver atoms were available, further growth of the nucleus was possible, and thus made the silver nanoparticles grow larger.

After the silver nanoparticles been synthesized in aqueous suspension, as they would be mixed with bacteria in the later experiment, post-treatment should be applied. Since this colloidal suspension could not suffer high temperature autoclave (120^{o}C, 15 minutes), centrifugation and filtration were employed. The centrifugation followed the same conditions mentioned in previous section; afterwards, the re-dispersed colloidal suspension was filtered using a Minipore filter, to get rid of potential bacteria inside the suspension. The filter possessed holes of 200 nm in diameter, which was small enough in regard of normal bacterial size. After the filtration, colloidal suspension was considered bacterial free, and was ready for the bactericidal test.

3.1.5. Measurement of Silver Nanoparticles' Zeta Potential

Silver nanoparticles' zeta potential was measured using ESA-9800 from Matec Applied Sciences. The measurement is based on the microelectrophoresis technique, which is the best-known method for the determination of particles zeta potential in colloidal suspension. Figure 3.2 is a schematic of the traditional microelectrophoresis technique.

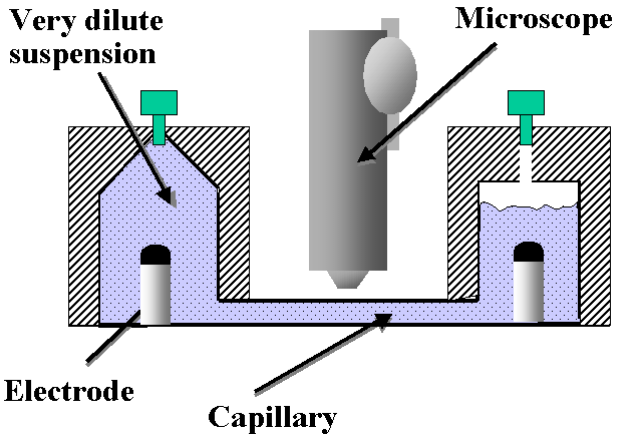

Figure 3.2: A schematic of microelectrophoresis measurement. The particles' zeta potential is determined and calculated by knowing the electric field generated by the two electrodes, and the velocity of the particles.

The apparatus includes a capillary cell, two chambers that include electrodes, and a means of observing the motion of particles. The apparatus is filled with a very dilute suspension of nanoparticles and the chambers are closed. A direct-current voltage is applied between electrodes in the respective chambers, to generate the electric field strength to be unit in the middle point of two chambers. One uses a microscope to determine the velocity of particles. The ratio of the velocity to the electrical field strength is known as the electrophoretic mobility. By making reasonable assumptions about the size of the observed particles and the electrical conductivity, it is possible to calculate the value of the zeta potential. Zeta potential values near to zero indicate that the particles in the mixture are likely to stick together when they collide, unless they also are stabilized by non-electrical factors. Particles having a negative zeta potential are expected to interact strongly with cationic additives.

For the measurement of the zeta potential of as-synthesized silver nanoparticles, 30 ml of diluted suspensions, about 5 mg/L of silver nanoparticles were used. Suspensions were adjusted to different pH value from 2 to 13, using 1 molar HCl and 1 molar NaOH. Each sample was then mechanically stirred for 15 minutes to reach the ionic equilibrium. During the measurement, particle velocity was dependent upon the electric field strength or voltage gradient, the dielectric constant and viscosity of the liquid, and the zeta potential. Smoluchowski's formula is widely accepted in the calculation of zeta potential.

$$\xi = \frac{4\pi\eta}{\varepsilon} \times U \times 300 \times 1000 \qquad (3.1)$$

Whereas ξ is zeta potential (mV), η is the viscosity of the solution, ε is the dielectric constant, $U = \frac{v}{V/L}$ is the electrophoretic mobility, v is the speed of the particle, V is the voltage applied to the two electrodes, and L to be the distance between the two electrodes.

3.2. Bactericidal Tests

Bactericidal tests were run after the synthesis of silver nanoparticles. The effect of silver nanoparticles on bacterial was considered as two aspects. One possible effect was the inhibition of bacterial growth, via the retardation of bacterial cell duplication; the other effect of the nanoparticles was the direct killing of bacterial cells, which may be the result of one or more mechanisms. Therefore, bacterial growth inhibition and cell killing must be distinguished from each other to guide us as we look for the bactericidal mechanism of silver nanoparticles on bacterial cells. However, these two effects were always found to be coupled since they were naturally linked together from biological point of view. In addition of the medium growth tests, bacterial viability tests were also applied to decouple these processes. Based on counting the live cells on agar surface and direct observation via fluorescence microscopy, we were able to measure the percentage of dead cells. A comparison of this data with the data derived from medium growth test may allow the actual effects of silver nanoparticles on bacterial cells recognized.

Chemicals and Cultures

LIVE/DEAD BacLight Bacterial Viability Kits L7007 was obtained from Molecular Probes, and stored in -40^{o}C before the fluorescence microscopic observation. The components of the Luria-Bertani (LB) medium, Tryptic Soy Broth[58], and agar solidifying powder were purchased from Difco Laboratories. *E. coli* RP437[59] and *S aureus* ATCC 12600 were obtained from Department of Biology, Virginia Tech.

3.2.1. Bacterial Growth Tests

In general, bactericidal effects could be divided into two types: 1) direct killing of the bacterial cells and 2) bacterial growth retardation. There is no indication to show which pathway is better than the other. It is quite reasonable for antibiotics to kill one kind of bacterium while they work to retard the growth of

bacteria on another kind of bacterium. In this regard, experiments were setup to distinguish which of these two mechanisms were initiated when silver nanoparticles were incubated with Gram-negative and Gram-positive bacteria.

Bacterial growth tests showed the overall effects of silver nanoparticles on bacteria. As mentioned before, two kinds of bacteria were used in this experiment, *E. coli* and *S aureus*. Since *E. coli* was one kind of gram-negative bacteria, while *S. aureus* was under gram-positive branch, it was expected to study the possibly different mechanisms involved with silver nanoparticles interact with two types of bacteria.

The experiment was conducted as follows. First of all, 10ml cultures of either *E. coli* or *S. aureus* were grown overnight, to the late log phase, in a nutrient broth, LB medium for *E. coli* and tryptic soy for *S. aureus,* respectively. As mentioned in Section 2.3.2, the bacteria are alive in the log phase, and the population was relatively large for study. Second of all, as the relative number of bacteria in interest also influenced the bactericidal effects, it was required to determine the cell numbers at the very beginning of the test and hold it constant for the beginning of each test. Therefore, after the bacteria were cultured, their optical density at 600 nm of a 1ml aliquot in acrylic absorption cuvette was determined. Based on a calculation, certain volume of cells was transferred to 50ml of nutrient medium, to make the starting optical density equals to 0.05. By doing this, the starting number of bacteria was around $2.5*10^7$/ml. This was a traditional method that is used by biologists to obtain a certain number of bacterial cells in a specific volume of media.

As for the third stage, the nutrient mediums were then mixed with silver nanoparticles. The concentrations of silver nanoparticles used were chosen from a range from 0 mg/L to 120 mg/L. Since silver nanoparticles also absorb light at 600 nm, about 1ml of each mixture, prepared before the addition of bacteria, were kept to determine the baseline of optical density. The bacteria containing mixtures were then cultured at 37^{o}C for up to 10 hours, the mixture was violently

stirred to keep the suspension uniformity. The optical density data were taken every 25 minutes for *E. coli* and 40 minutes for *S. aureus* as their usual generation time are different. From the optical density data, we could easily correlate the optical density into the number of bacterial cells. By studying the bacterial growth curve, we could identify whether or not the silver nanoparticles possessed strong effects on bacterial cells. Further tests should be done in order to clarify the specific effect.

3.2.2. Bacterial Viability Tests

Agar Plate Test

To determine whether silver nanoparticles could kill the bacteria or cause the growth retardation, agar plate test was executed. In this test, bacterial cells were separated from the nutrient medium by centrifugation and were then suspended in ionic PBS[60] buffer right after the culture phase. Because of the ionic potential that PBS buffer built outside the bacterial cell wall, the bacteria were kept in a balanced potential and would stay alive. Otherwise, the internal ionic potential would cause the bacterial wall to explode, resulting in natural cell death. By transferring the bacterial cells into PBS buffer that contained no nutrients, they would not have population growth afterward transfer, in other words, the number of bacteria cells were kept constant. After the washing process, 2.5ml of bacteria were transferred to test tubes. The optical density was adjusted to 1.0 by the addition of buffer solution.

A matrix of experiments was conducted to determine the effect of the concentration of silver nanoparticles on the cells. The silver concentration was calculated by assuming all the silver ions were reduced into atoms and thus formed the colloidal silver particles. Ionic buffer solution was added to adjust the total volume to be 5ml. By this means, the optical density of bacteria was actually 0.5 since we doubled the volume of the suspension. These silver-bacteria mixtures were then cultured in 37^{o}C with continuous shaking for 3 hours

before series of dilution were done, and the bacteria cells were plated on the surface of agar plates. The procedure could be detailed as follows.

1. 15ml of cultured bacteria (either *E. coli* or *S. aureus*) were concentrated by centrifugation at 10,000 g for 15 minutes;
2. Remove the supernatant and resuspend the pellet in 1ml of autoclaved potassium phosphate buffer (pH 7.4);
3. Add the 1ml suspension to 30ml centrifuge tube, which contained 20ml of potassium phosphate buffer;
4. Incubate the bacteria at room temperature for 1 hour, mixing every 15 minutes;
5. Pellet the suspension by centrifugation at 10,000 g for 15 minutes;
6. Resuspend the pellet in 20ml of potassium phosphate buffer, and then centrifuge again;
7. Resuspend the pellet in 10ml of potassium phosphate buffer;
8. Dilute the bacterial suspension with potassium phosphate buffer, until the optical density at 600nm was measured to be 1.0, and transfer 2.5ml of such diluted suspension to each of testing tubes. Since we chose four different concentrations of silver nanoparticles to test and tested each concentration 3 times, the total number of testing tubes would be 12;
9. Colloidal silver nanoparticles were then mixed with the bacterial suspension. Since all silver nanoparticles came from the same stock suspension, their final concentration would be determined by the amount of the volume. Potassium phosphate buffer was used to adjust the total volume to be 5.0ml;

	E.coli/Staphy.aureus	Colloidal silver	PBS
A (Control)	2.5ml	0	2.5ml
B (120mg/L)	2.5ml	2.5ml	0
C (60mg/L)	2.5ml	1.25ml	1.25ml
D (30mg/L)	2.5ml	0.83ml	1.67ml

10. Culture the mixtures at 37^{o}C with shaking for 3 hours;
11. Dilute the cultured suspension for 20,000 times with potassium phosphate buffer, to get the first "plate concentration" (~1.25*10^{4} cell/ml). Afterwards, two times ten-fold dilution were executed, thus obtain the second and third plate concentration of 1.25*10^{3} cells/ml and 1.25*10^{2} cells/ml, respectively. These three concentrations were recorded as concentration "1", "2", and "3", for ease of recording and tracing;
12. Place 250ul of each suspension on the surface of agar plates with the help of glass beads.

These agar plates were then stored in a warm room (37^{o}C) overnight for the formation of bacterial colonies. As is well known, live bacterial cell would absorb nutrients and eventually expand in size and form a bacterial colony after certain period of time. For the dead cells, nothing was expected to happen. Therefore, by counting the number of bacterial colonies formed afterwards, we could determine the ratio of bacteria, which were alive after the treatment with silver nanoparticles. This was crucial in judging the bactericidal effects of silver nanoparticles.

Fluorescent Microscopic Observation

As an alternative method to determine the bacterial viability, fluorescence microscopy experiment was carried out. Basically, it shared the same sample preparation procedure with the nutrient agar test. Instead of placing on the agar surface after the mixture being cultured for 3 hours, they were firstly centrifuged to remove the silver nanoparticles because we did not want the silver nanoparticles to continue to affect the bacteria during the fluorescence observation. Suspensions were then mixed with the LIVE/DEAD bacterial viability molecular dyes and stored in dark for 15 minutes. Based on recognizing the bacterial membrane integrity, intact membrane for live bacteria and damaged

membrane for dead bacteria, these dyes fluorescence at different wavelengths of light, typically green for live cell and red for dead cell. Therefore, the fluorescence microscopic images could be used as direct proof to determine the effects that silver nanoparticles had on the bacteria. Texas Red bandpass filter sets were applied during the fluorescence microscopic observation. By changing the filters, light with different wavelength other than red or green would be filtered and, thus, the corresponding microscopic image would only showed as green or red.

Briefly, 6ul of stained bacterial suspension were trapped between a slide and a 24 mm square coverslip. Using an oil emersion lens, optimal magnification could be chosen. During the course of observation, filters could be changed. At each spot of interest, two images were taken, with one image showed all the cells in the spot, while the other one showed only the dead cells. Based on simple comparison of these two images, numbers of dead cells and live cells could be counted easily via software, like Image-Pro Plus. In view of demonstration, cells were tinted manually, as red for dead cells, and green for live cells. Afterwards, two images were merged together. Since the dead cells showed in both images, during the image merging, based on the intensity of two images, lots of cells were displayed as either yellow or brown. As a consequence, these cells should be considered as dead cells. After the cell numbers had been counted, the proportion of dead cells could be calculated.

CHAPTER 4.
Results

4.1. Characterization of Silver Nanoparticles

Silver-anchored silica nanoparticles are synthesized by the surface modification method via tin sensitization and silver activation of the silica nanoparticles. Nanoscale silica suspension serves as a heterogeneous nucleation and stabilization medium. Silver particles are directly adsorbed onto the silica surface by the reduction and deposition processes, with controllable diameter from 2-nm to 20-nm. This nanostructure takes advantage of silica nanoparticles as steric barrier as well as the strong electrical repulsive force that silica particles posses, thus the resulting colloidal suspension has a great enhancement in the stability. These silver-silica nano-composites were then characterized carefully, where ultraviolet-visible scanning spectroscopy was used for determining the colloids' optical absorption spectrum and transmission electron microscopy (TEM) was employed from the morphology and particle size point of view.

4.1.1. UV-vis Absorption Spectrum

Optical absorption spectra of the silver-silica nano-composites suspensions were obtained with a Shimadzu UV-3101PC UV-vis-NIR scanning spectrometer, shown as Figure 4.1, in the wavelength range from 300 nm to 700 nm. Quartz cuvettes with optical path length of 10 mm were used in the measurements.

Figure 4.1: Shimadzu UV-3101PC UV-vis-NIR scanning spectrometer.

Typically, to exclude the background absorption spectrum, equipment was first calibrated with a blank sample of the chosen solvent. The sample is placed into the cuvette and is hold in the spectrophotometer sample chamber. A pulse of wide-spectrum light, generated by a tungsten bulb, is passed through the sample and the resulting absorption is collected and the blank sample is subtracted out.

As described in former section, metallic nanoparticles would show distinct absorption spectrum when suspended in aqueous suspension. Theoretically, colloidal silver nanoparticles, with dimension below 30 nm, possess optical spectrum with absorption peak, also known as the surface plasmon resonance (SPR) peak, lies ~400 nm. Figure 4.2 shows one bottle of typical silver nanoparticles, with clear, bright yellowish color. The full width at half maximum (FWHM), is typically around 50~60 nm. From the absorption spectrum taken on the as-synthesized silver-silica nano-composites, Figure 4.3, it was clear that the distinct absorption spectrum of silver nanoparticles had not been disturbed by the silica nanoparticles mixed in the suspension. Both the absorption peak and the FWHM were in accordance with the normal pure silver nanoparticles[61].

Figure 4.2: Synthesized silver-silica nano-composites dispersed in DI water. Due to the distinct absorption of light at ~400 nm, the suspension shows a clear, bright, yellowish color. If the silver concentration is increased, the suspension is expected to have relatively darker color.

The colloidal silver suspension shows yellow in color, which could be easily explained from the optical properties of silica nanoparticles point of view. Silica nanoparticles were basically optical transparent, which would not have special light absorption across the whole spectrum. However, since the dielectric constant of silica is different from the solvent, H_2O in this case, light scattering will happen to some extent. Parallel experiments had been done by mix silica colloids into the silver nanoparticle suspension, which made the suspension looked turbid. The effect on the absorption spectrum was a background signal associated with the scattering that was convolved with absorption peak associated with the Ag nanoparticles, obscuring the surface plasmon resonance peak Both absorption spectra increased to some extent at the short wavelength end. Images are not presented here.

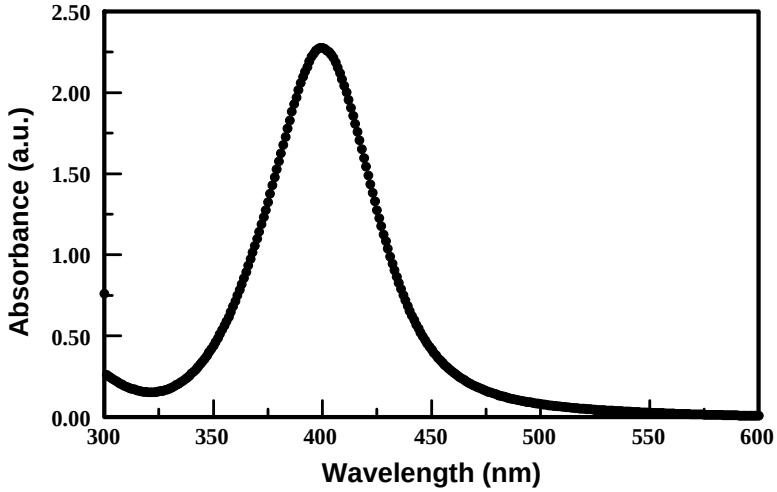

Figure 4.3: UV-vis absorption spectrum of silver-silica composite nanoparticles. The spectrum is identical to pure silver nanoparticles, with absorption peak at 400-nm, and FWHM around 50-nm. Therefore we concluded that silica nanoparticles would not affect the optical properties of silver nanoparticles, except background light scattering all over the spectrum.

4.1.2. TEM Images

Transmission electron microscopy (TEM) investigation of silver-silica nano-composite nanoparticles is a direct and effective approach to determine the particle size and morphology of the nanoparticles, as well as the dispersion uniformity.

During the operation of TEM, an electron beam is focused on a thin layer of dried nano colloids, which were deposited on a 200 mesh copper grid coated in carbon. Electrons pass through the particles at a slower rate than through the carbon grid due to the difference in atomic electron density and have an increased chance of scattering. Therefore, by collecting the number of electrons, the electron sensor is able to identify the high-density area from the overall background. Particles with high density will appear darker in the TEM negative

films, and in our case, silver nanoparticles are the darkest ones, and silica nanoparticles are a little bit lighter.

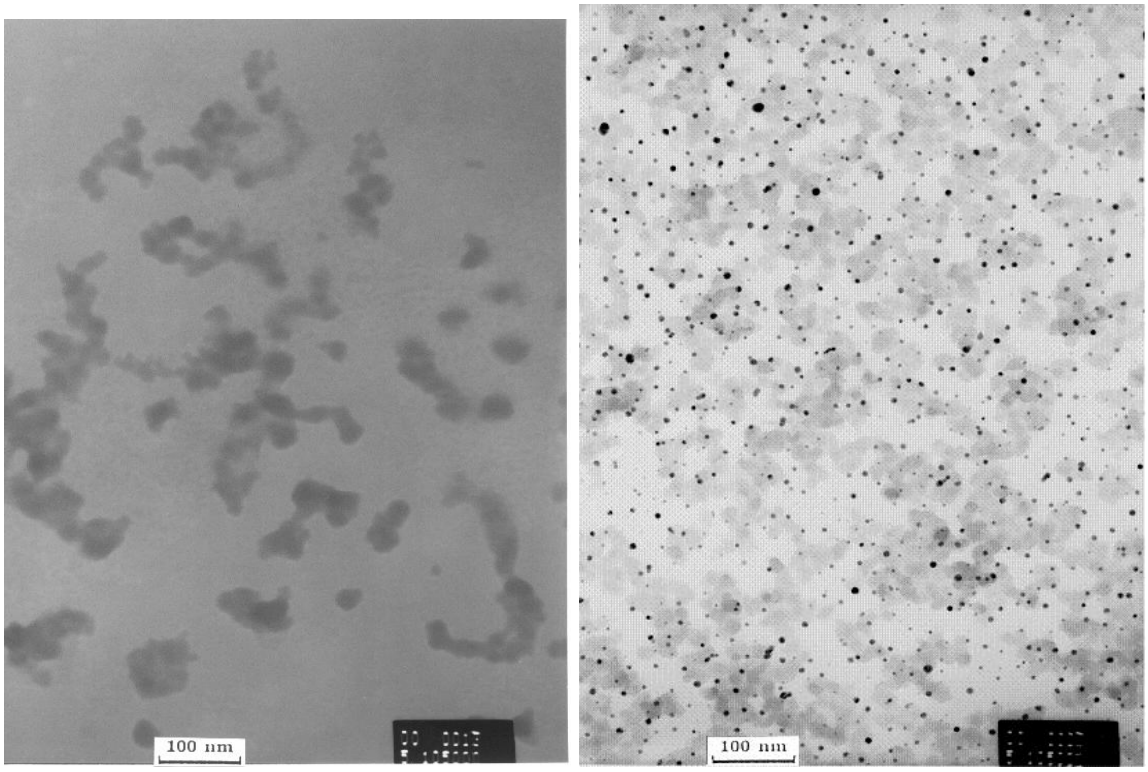

(A) **(B)**

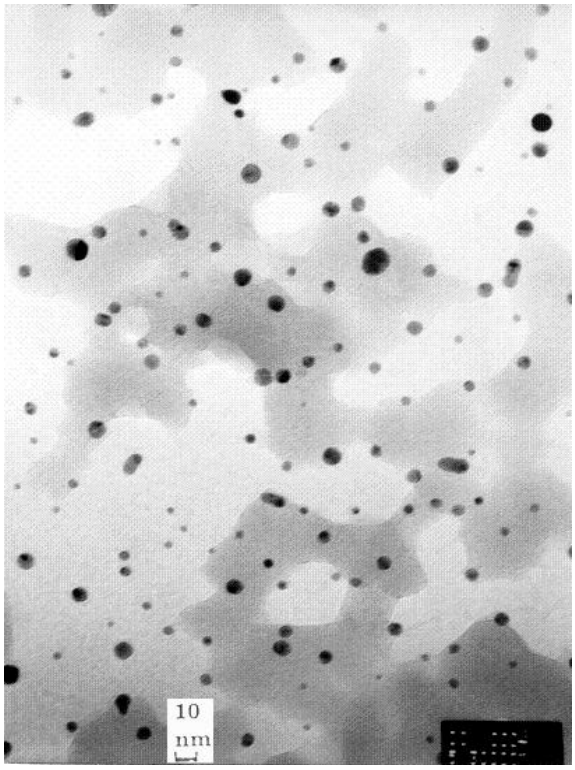

(C)

Figure 4.4: TEM images of silver-silica nano-composites. (A) Commercial silica nanoparticles used in this project, with mean diameter of 14 nm. (B) Silver-silica nanoparticles. As observed, most of the as synthesized silver nanoparticles were spherical, with particle size about 5 nm in diameter. The image magnification is 105,000. (C) Silver-silica nano-composites, it is the same sample with B. The image magnification is 300,000.

Figure 4.4(A) illustrated the TEM image of commercial silica nanoparticles used in this project. These silica nanoparticles were of extremely stable with high concentration, 40-wt% in H_2O. Because of the low optical density of these silica nanoparticles as well as their small size, individual particles were not very distinguishable under the TEM scope. However, particles could still be identified through careful observation.

Figure 4.4(B, C) depicted the silver-silica nanoparticles synthesized in this project. (B) and (C) were taken from the same sample at different

magnifications. The as-reduced silver nanoparticles were attaching on the silica surface, although some of the small ones were also found de-attached for some reason, the coupling structure was basically achieved. In regard of the particle size distribution, most of the silver nanoparticles were varying between ~2 nm and ~6 nm. As claimed in previous section, the particle size distribution was not of extremely important in this project since we only aimed to investigate the bactericidal effects of silver nanoparticles. The influence of particle size might be considered as another issue in the future research.

4.1.3. Measurement of Zeta Potential of the Silver-Silica Nano-Composites

The stability of the silver-silica nano-composites was determined by measuring the colloids' zeta potential. The suspension's pH was pre-titrated from 2 to 12, which covered the biologically relevant pH range. Ten measurements were taken for each sample, and their average numbers were considered to be true value of the sample for the specific pH. Standard deviations were also calculated, showing the relative accuracy of each measurement. Table 4.1 listed all the measurements, as well as the calculated standard deviations.

Table 4.1: Zeta potential of the silver-silica nano-composites versus different pH values. Particle mobility was the raw observable of the equipment. The zeta potential data were then calculated using the average from ten velocity measurements.

Sample pH	Particle Mobility (inch/min)	Zeta Potential (mV)	Standard Deviation (mV)
2	2.07	28.8	1.3
3	2.45	36.2	0.5
4	0.65	8.9	0.7
5	1.22	-1.7	0.6

6	-0.82	-11.4	0.5
7	-1.86	-25.8	0.9
8	-3.324	-46.2	0.4
9	-3.50	-48.7	0.5
10	-3.74	-52	0.3
11	-3.39	-47.2	1.2
12	-3.28	-45.6	1.5

4.2. Results of Bactericidal Tests

Bactericidal tests were conducted as described in previous section. For each set of tests, bacterial medium growth test and bacterial viability test, at least three parallel tests were conducted to obtain reliable results.

As silica nanoparticles are chemically inert and biological benign, they are not supposed to bring any effects to the bactericidal tests, which is also been confirmed from our experimental data. The sample with the mixture of colloidal silica and all of the chemicals, except the silver component, showed no bactericidal effects at all. Samples containing silver nanoparticles possessed strong influence to bacterial viability and duplication ability, both on *E. coli* and *S. aureus*. Therefore we concluded that the bactericidal effects of this nano-composite were only due to the silver nanoparticles.

4.2.1. Bacterial Medium Growth Curves

For the medium growth test, number of bacteria was determined by recording the bacterial optical density. Genesys 10 UV-vis spectrophotometer was used in the measurements of the optical density of the bacterial cultures in liquid nutrient medium, with the measuring wavelength set at 600 nm.

The optical density of a bacterial culture is a measurement used by microbiologists to determine the number of bacterial cells present in a liquid

culture. As introduced in section 2.3.2, growth of bacteria could always be considered as four distinct phases, namely, lag phase, exponential phase, stationary phase, and death phase. However, the lag phase, stationary phase, and death phase were to some extent related to many environmental conditions, such as temperature, nutrient concentration, and etc. Therefore, we considered the exponential phase to be the phase of interest in this project since it provided most the information concerning the bacteria themselves. From the study of the curve slopes of exponential phase, we are able to calculate the bacterial generation time, which gave us a general idea as to whether or not the silver nanoparticles have any significant effect on bacterial cells.

Escherichia coli

Results of the medium growth tests of *E. coli* were depicted in Figure 4.5, where optical density was taken every 30 minutes. With different proportion of silver nanoparticles, the bacterial growth curves showed significant differences across the whole four phases. When we increase the concentration of silver nanoparticles from 0-mg/L to 60-mg/L, the bacterial optical density decreased significantly. In the 60-mg/L sample, a barely observable increase in bacterial optical density was observed, indicating that only a small portion of bacteria was still duplicating, while all of the rest of the bacteria were killed or their growth was inhibited.

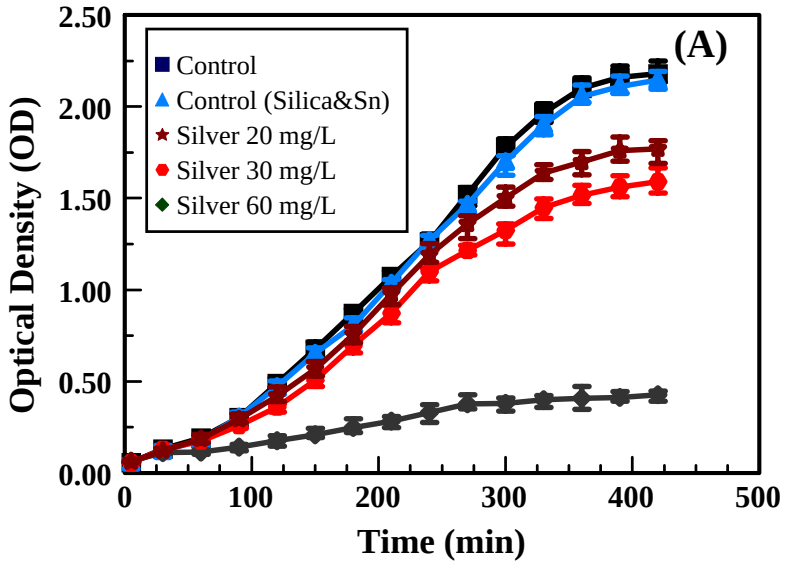

Figure 4.5: Bacterial growth curves of *E. coli* (optical density versus time).

As discussed in section 2.3.2, the exponential phase of the bacterial growth is the most informative stage. Therefore, six consecutive points were selected as the representatives of exponential phase, as were depicted in Figure 4.6.

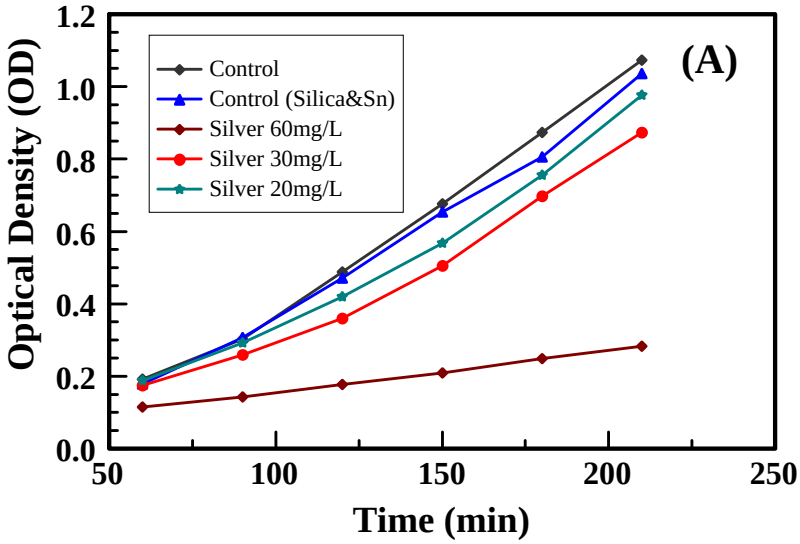

Figure 4.6: Exponential growth phase of *E. coli* (cell number versus time). Six consecutive points were selected purposely.

Since the relation between optical density and the cell number is not linear, the coordinate should be changed to an exponential scale to obtain a linear correspondence to the actual cell numbers. As optical density of 1.0 at 600 nm usually corresponding to $5.0*10^8$ cells per milliliter, we can calculate the number of cells by multiple the as-measured optical densities with this coefficient, which was a constant. Figure 4.7 illustrated the bacterial growth curves of *E. coli* with exponential coordinate, which directly corresponds to cell number. In regard of the influence on generation time, which could only be determined from the exponential phase, several points were selected and were considered as the points in exponential phase. The significant discrepancies of these curves could still be identified, especially on the samples with high silver concentration. Bacterial growth rate as well as generation time could be derived from the linear curve fittings of these points.

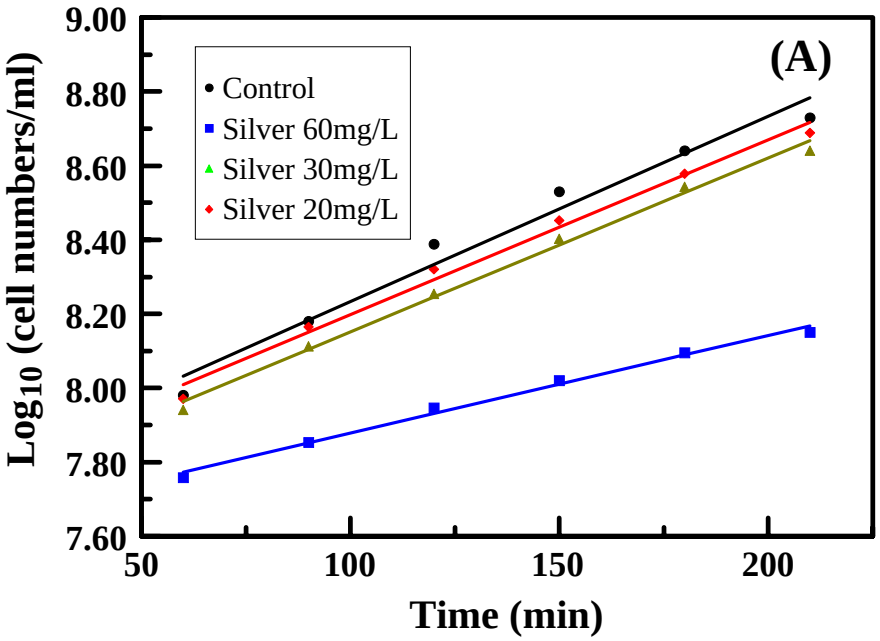

Figure 4.7: Exponential phase of *E. coli.*

As illustrated in Figure 4.7, six consecutive points were chosen as the exponential growth phase data. The cell numbers in the control sample and the sample with 30 mg/L silver nanoparticles increased at almost the same rate,

while the number of cells in the sample with 60-mg/L silver nanoparticles increased at much smaller rate, which indicated that the bacterial growth had been retarded to some extent or even some of the bacteria been killed when exposed to the high concentration of silver nanoparticles. Samples with 20-mg/L and 30-mg/L silver nanoparticles have almost identical rate of growth as the control sample. **Table 4.2** showed the growth rate of the exponential growth phase of *E. coli*.

Table 4.2: Curve slopes of the exponential phase of E. coli versus the concentration of silver nanoparticles.

	Concentration of Silver Nanoparticles (mg/L)			
Bacteria	**0**	**20**	**30**	**60**
E. coli growth rate (generation/min)	0.0050	0.0047	0.0046	0.0026

S. aureus

Gram-positive bacteria were much more difficult to kill, due to the quite different cell wall structure as compared to Gram-negative bacteria. We purposely increased the concentration of silver nanoparticles used in this set of tests. Instead of 20, 30, and 60-mg/L used in *E. coli* test, the silver concentrations were 30, 60, and 120-mg/L for *S. aureus.* The same experimental procedures had been applied on *S. aureus* with the only other parameter that different from *E. coli* test was the time interval of the optical density measurements. Since the normal generation time of *S. aureus* was 27~35 minutes under optimum conditions, we chose to take the optical density every 40 minutes. The data is presented in Figure 4.8.

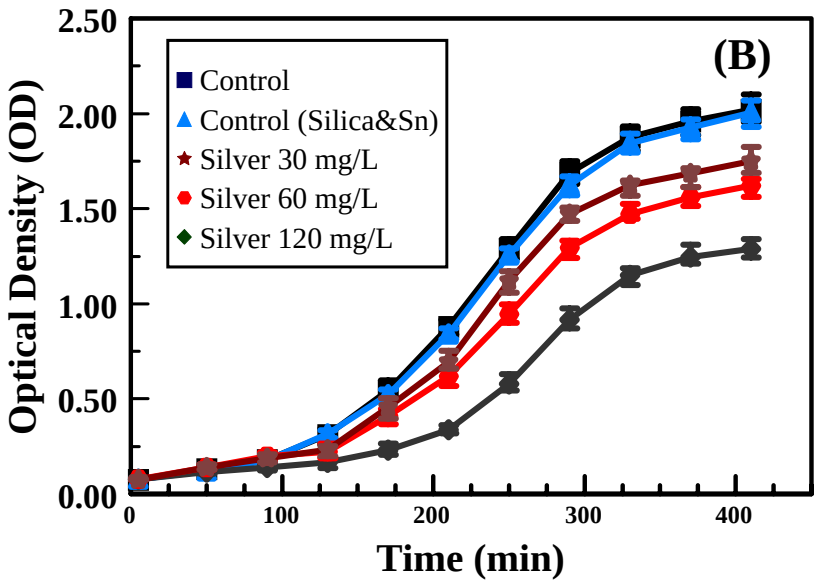

Figure 4.8: Bacterial growth curves of *S. aureus* (optical density versus time).

Results of medium growth optical densities had been collected on *S. aureus*. The differences between the control sample and the silver-contained samples became larger as we increased the silver concentration. However, the differences were not that significant when compared with the effects on *E. coli*. Obvious changes could only be observed when the silver concentration was increased to 120-mg/L, which was twice the maximum concentration used in *E. coli* tests. When we changed the coordinate to exponential scale and focused on study the exponential phase of bacterial growth, only slight differences between the control sample and the silver-contained samples could be detected, in regard of the cell number and bacterial growth rate. Figure 4.9 and Figure 4.10 depicted the points in the exponential phase, and the corresponding points in exponential coordinates.

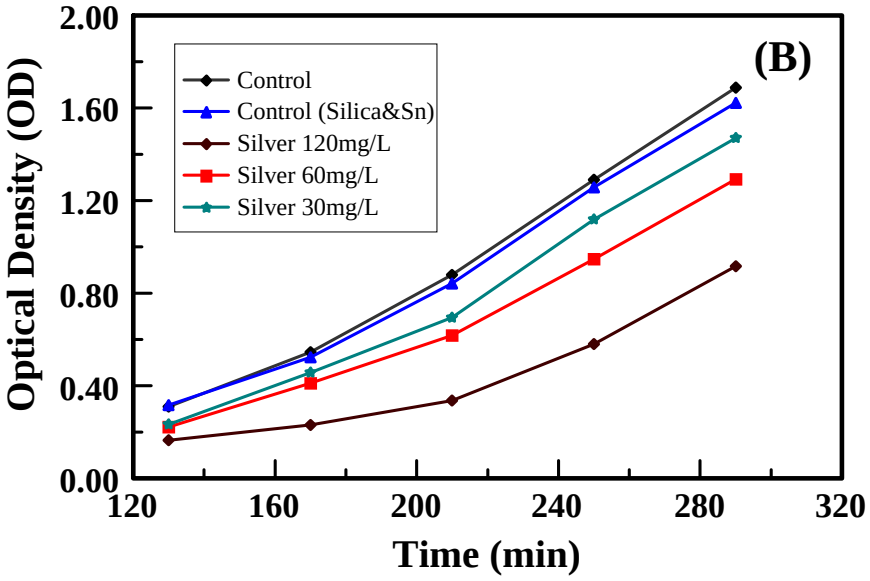

Figure 4.9: Bacterial growth curves of *S. aureus* (cell number versus time).

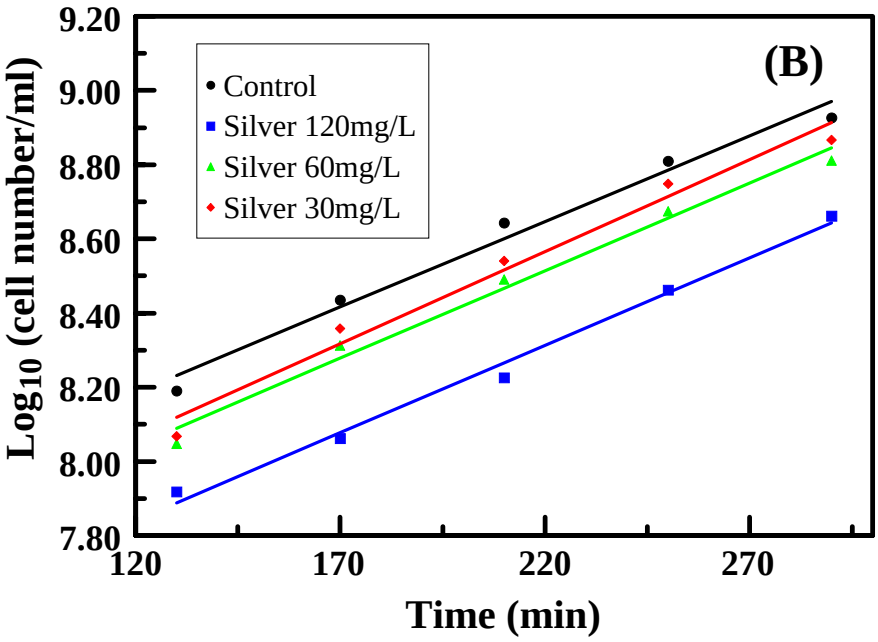

Figure 4.10: Exponential phase of *S. aureus.*

As we calculate the slopes of the as-derived curves, which were showed in **Table 4.3**, the data were amazingly close to each other, corresponding to no

obvious change in the bacterial generation time. Hence, we had the impression that the silver nanoparticles might only kill some of the *S. aureus* cells, rather than inhibited the bacterial growth.

Table 4.3: Curve slopes of the exponential phase of *S. aureus* versus the concentration of silver nanoparticles.

	Concentration of Silver Nanoparticles (mg/L)			
Bacteria	**0**	**30**	**60**	**120**
S. aureus growth rate (generation/min)	0.0047	0.0048	0.0047	0.0047

4.2.2. Bacterial Viability Determination

Based on the data derived from the liquid medium tests, we were able to see that the bacterial cell number was dropped tremendously in both types of bacteria. However, from the data on bacterial generation time, silver nanoparticles possessed quite different effects on them. Therefore, we were interested in finding out whether the bacterial cells were really been killed by silver nanoparticles, or just their duplication ability been limited. This required evidence of the bacterial viability after the treatment of silver nanoparticles. Two techniques were used to determine bacterial viability after several hours' treatment with the silver nanoparticles, agar plate tests and fluorescent microscopic observation. Significant differences could be recognized while comparing the bactericidal effects of silver nanoparticles against *E. coli* with *S. aureus*.

Escherichia coli

As described earlier, bacteria were placed on the agar surfaces with different dilutions. We observed that an immediate coagulation occurred upon

addition of colloidal silver nanoparticles to any culture of bacteria, based on the changes of color of the mixture. This was due to the surface charge attraction between bacterial cells and the silver nanoparticles. In addition, change of colloidal environment may destroy the ionic charge equilibrium of silver nanoparticles and cause the particle coagulation to some extent.

For *E. coli*, as the medium growth tests were conducted before this bacterial viability test, we made assumption that a silver concentration of 60 mg/L was high enough in killing most of the bacterial cells based on previous results. Therefore, we focused our attention on silver concentrations of 60-mg/L, 30-mg/L, and 20-mg/L. After three hours' inoculation with silver nanoparticles at 37^{o}C, 250 µl silver-containing bacterial suspensions were transferred to the agar plates using a micropipette. With the help of glass beads and with mild vibration, the suspension spread evenly over the surface. All of the agar plates were then stored in a warm room (37^{o}C) overnight to allow the formation of bacterial colonies. The numbers of colonies were counted via Image-pro Plus.

Parts of the agar plate images were presented below. Figure 4.11(A) and (B) were the images of the control samples with different bacterial concentrations, around 3000 cells/plate and 300 cells/plate respectively, as described in the experimental section. (C) was the image taken from the sample with highest silver concentration, 60-mg/L. There was no colony formed on the agar; however, we did find a very small number of colonies in other samples with the same bacterial and silver nanoparticle concentration, duplicates that were used to verify the data. It should be clear that almost all the bacterial cells were killed under the influence of this concentration of silver nanoparticles.

(A)

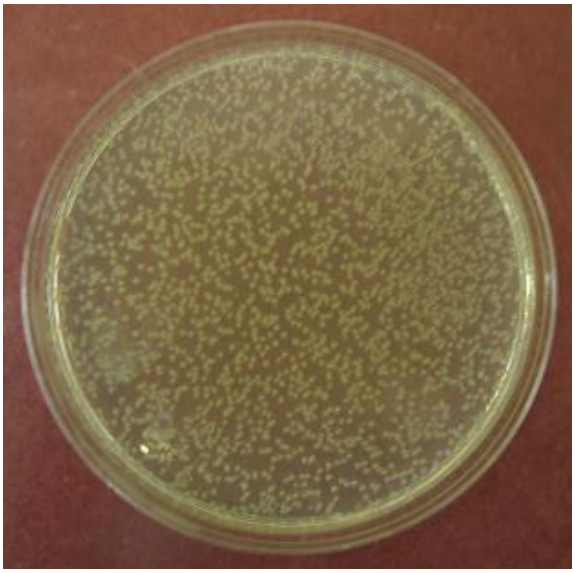

(B)

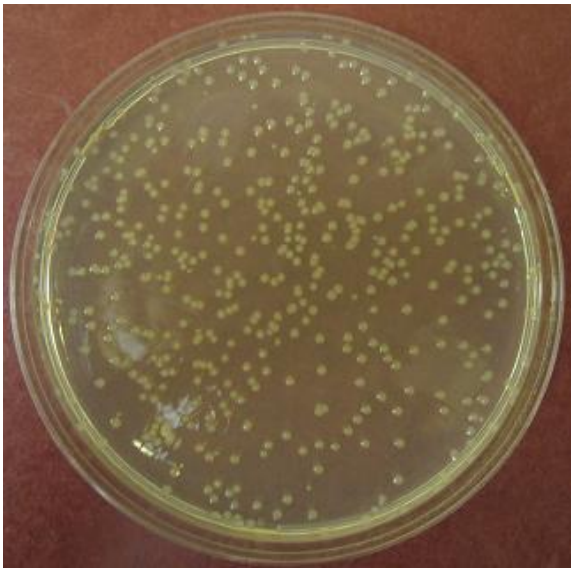

(C)

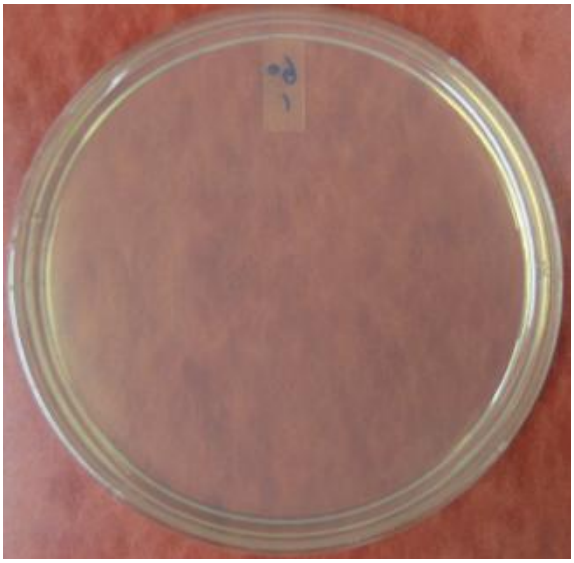

(D)

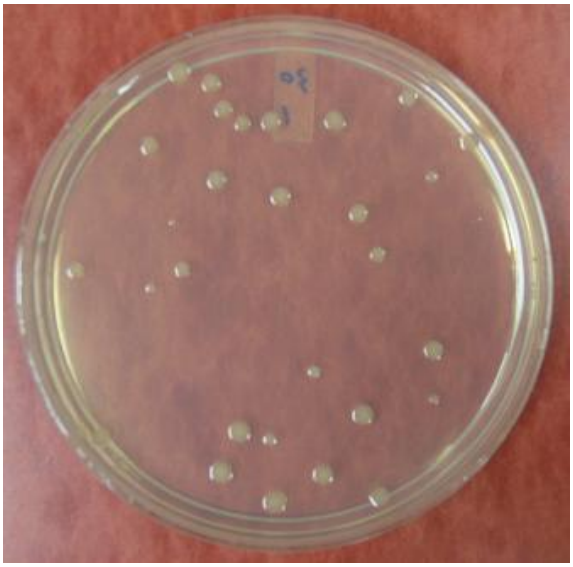

(E)

(F)

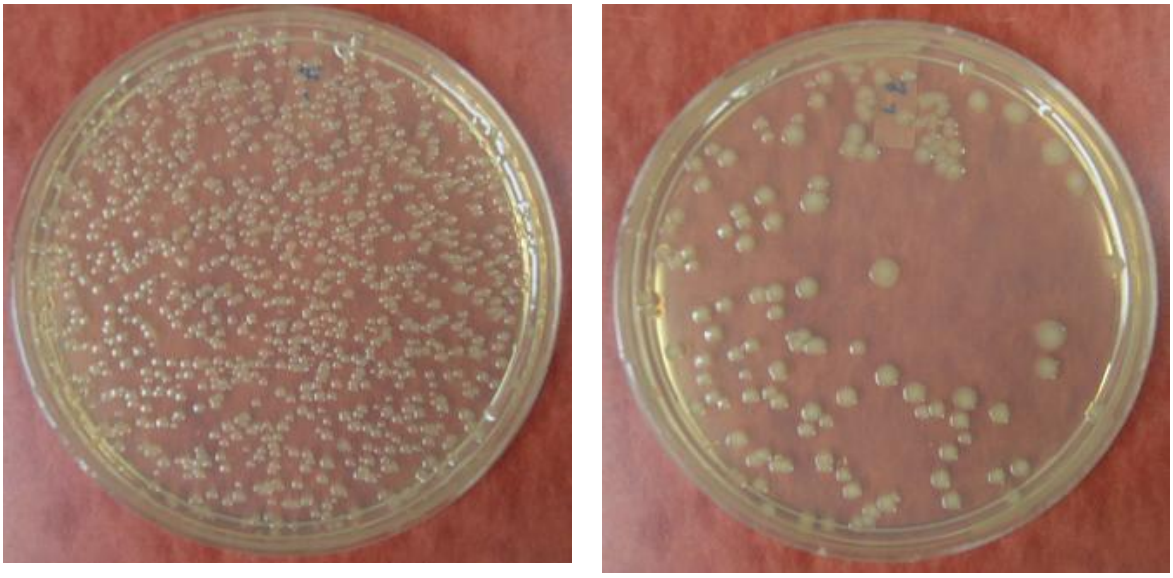

Figure 4.11: Agar plate images of different concentration of *E. coli*, as well as different concentration of silver nanoparticles. (A) and (B) Control samples, with *E. coli* concentration of 3000 cells/plate and 300 cells/plate, respectively. The bacterial colonies in sample A were too crowding to count because many of them were actually overlapped due to the limited space. (C) Sample with *E. coli* concentration 3000 cells/plate, and highest silver concentration, 60 mg/L. No colony was found in this specific sample, although we did observe bacterial colonies on other parallel samples, which were treated under exactly the same condition. (D) Sample with *E. coli* concentration 3000 cells/plate and silver concentration of 30-mg/L. Several colonies were observed, which was still a very small portion. (E) Sample with *E. coli* concentration 3000 cells/plate, and silver concentration of 20-mg/L. Lots of colonies were formed in this sample, indicated that this low concentration of silver nanoparticles might have little effect on *E. coli* while the bacterial concentration was at this level. (F) Sample with *E. coli* concentration of 300 cells/plate, and silver concentration of 20-mg/L. Compared with the control sample although some colonies were formed, there was a significant reduction in the colony number.

However, when we keep the bacterial at 3000 cells/plate, and lower the silver concentration to 30-mg/L, a small number of colonies were observed after three hours' inoculation, as showed in (D). Therefore it was reasonable to draw

the conclusion that only a small proportion of *E. coli* were remained alive. After counting the as-formed bacterial colonies, this number was presented in the Table 4.4 showed below.

As we further lowered the silver concentration to 20-mg/L, significant changes occurred. Both (E) and (F) contained silver concentration of 20-mg/L, while (E) had a bacterial concentration of 3000 cells/plate, and (F) with bacterial concentration of 300 cells/plate. Unlike the samples showed in previous samples, (C) and (D), lots of colonies grew in (E), indicating that there was a weak influence of silver nanoparticles on the *E. coli* at this low concentration. In the sample with lower bacterial concentration, 300 cells/plate, as shown in (F), some colonies could still be found.

Table 4.4: Numbers of colonies formed on agar plates, overnight.

Concentration of silver nanoparticles	*E.coli* concentration ~3000/agar	*E.coli* concentration ~300/agar
0 mg/L (control)	N/A	279 ± 16
20mg/L	N/A	27 ± 18
30mg/L	54 ± 23	~0
60mg/L	12 ± 4	~0

An alternative approach in determining the bacterial viability is fluorescent microscopy. Detailed procedures could be found in section 3.2.2, which differed from agar plate tests only after the post-inoculation stage. Several centrifugations were carried out on all the bacterial suspensions, to simplify the fluorescent observation as well as to wash away the silver nanoparticles. After the centrifugation process, fluorescein was mixed with the bacterial suspensions, which were then and stored in dark for 15 minutes to allow sufficient attachment of fluorescein to bacterial cells.

As discussed in the experimental section 3.2.2, under certain conditions of excitation, fluorescein would fluorescent at one of two different wavelength – the specific wavelength depends on the intactness of bacterial cell walls. Therefore, the live and dead cells could be effectively identified based on the fluorescent light. In the typical experiment, live cells would fluoresce with a green emission wavelength while dead cells would appear as red. Hence, when images were taken at the same spot with different bandpass filter, we were able to distinguish dead cells from the live ones. Numbers of cells could be calculated via software such as Image-pro Plus.

Since there was no available filter to allow the collection of only the green emission from the live cells, the cell was stained as green during the analysis stage. Therefore, when the images were merging together to illustrate the overall image, the color of dead cells would be the addition of red and green. I.e., it would change to yellow or brown, based on the fluorescent intensity of the fluorescein at each cell. Figure 4.12 depicted these fluorescent microscopic images taken on the *E. coli* samples.

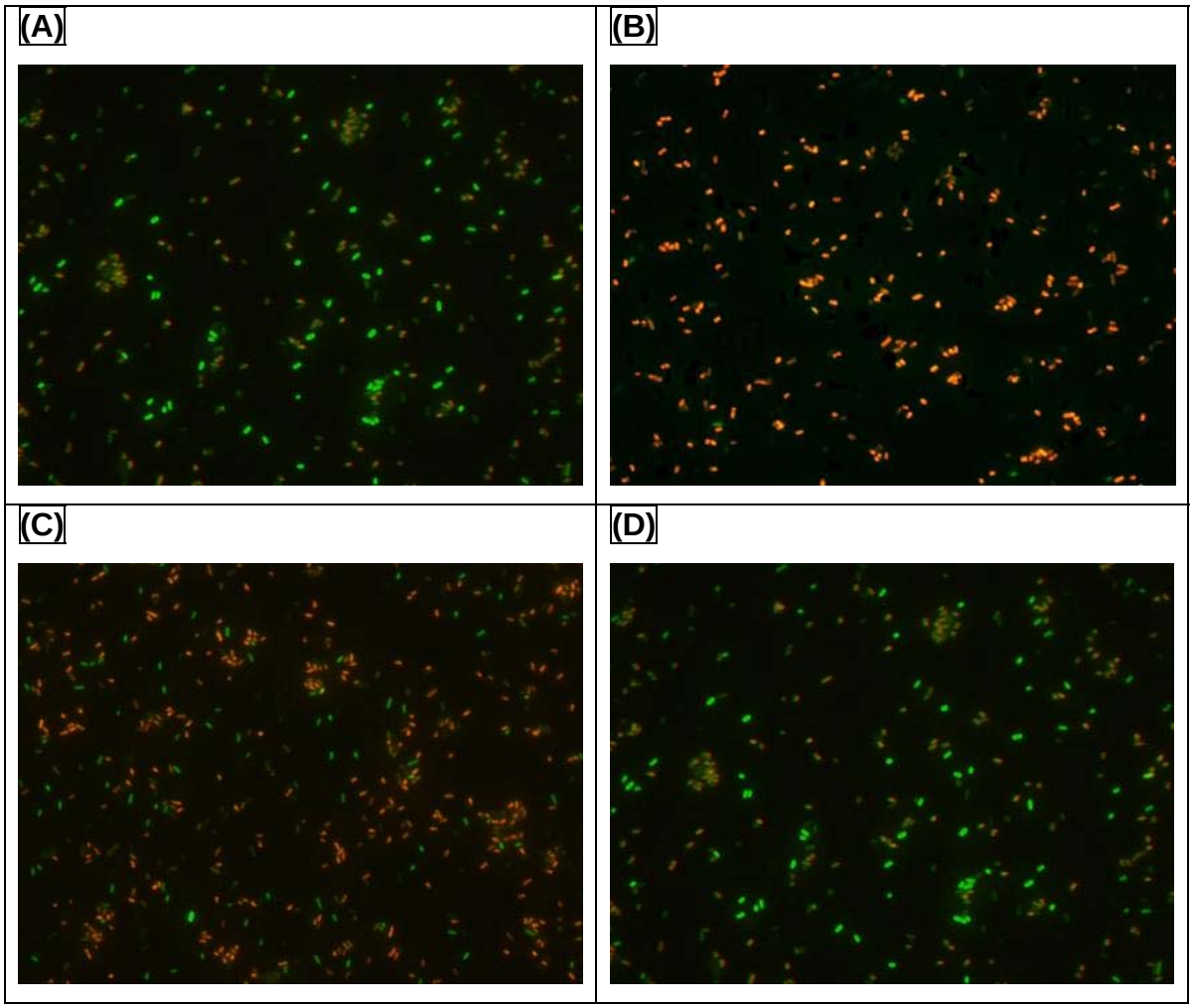

Figure 4.12: Fluorescent microscopic images of *E. coli* samples with different concentration of silver nanoparticles. (A) Control sample, with no addition of silver nanoparticles. As can be seen, almost all the cells were a green color, indicating that the experimental technique was basically correct. (B) Sample with highest silver concentration, 60-mg/L. The bacterial cells in this image were almost showed as yellowish or brownish. As discussed in previous experimental section, the images were generated by merging two images, while the dead cells were green in the overall image and red in another, they would supposed to be yellow or brown, depending on the specific optical density we used when the images were taken. (C) Sample with silver concentration of 30-mg/L. Again, like the case in sample with 60-mg/L, most of the cells were brownish or yellowish. (D) Sample with silver concentration of 20-mg/L. Some cells remained green, while most of them were still brownish.

As illustrated above, image (A) was taken on the control sample, which was used to prove the correctness of our experimental operation. The cells in this image were all green, indicating that they were all alive when the Fluorescein was added to the cell culture. When we increased the silver concentration to 60-mg/L, almost no green fluorescence from the cells could be found in (B), indicated that the majority of bacteria had been killed during the silver nanoparticle inoculation stage. Analogous to the case in sample (B), only a little bit more green fluorescence could be observed in (C). While (D) display a larger proportion of live cells compared with the former two samples. Cell numbers were calculated and depicted in **Table 4.5**. Therefore, in connection with the previous agar plate tests, both bacterial viability tests on *E. coli* showed excellent agreement with each other.

Table 4.5: Number of live and dead cells in different samples, *E. coli,* showed that most of the bacterial cells been killed when the silver concentration was greater than or equal to 30-mg/L.

Sample	Live	Dead	Live %
0 mg/L (control)	455	<5	~ 100 %
20 mg/L	82	433	15%
30 mg/L	28	374	7%
60 mg/L	<10	398	< 3%

Staphylococcus aureus

The bacterial viability tests on *S. aureus* followed the exact procedures as described in *E. coli* section. Both agar plate test and fluorescent microscopic observation were carried out.

Agar plate images were depicted in Figure 4.13. (A) and (B) were the images of two control samples, while (A) had the bacterial concentration of 3000 cells/plate; and the bacterial concentration in (B) was ten times more diluted, 300

cells/plate. Image (C) was taken from the sample with silver concentration of 60 mg/L as well as highest bacterial concentration, 3000 cells/plate. There were a large number of colonies. Image (D) was the sample with silver concentration of 60-mg/L and the bacterial cells were 300 cells/plate. A small portion of colonies was formed after plating. In comparison with sample (B), the number of colonies formed in (D) had been reduced significantly. However, when the silver concentration was raised to 60-mg/L and the bacterial concentration was kept at 3000 cells/plate, (showed in image (E)), only a few colonies were formed, indicated that the bactericidal property of silver nanoparticles were good for this concentration. As we reduced the number of bacterial cells to 300 cells/plate and at the concentration of 60-mg/L of silver nanoparticle, few colonies were observed, as showed in image (F).

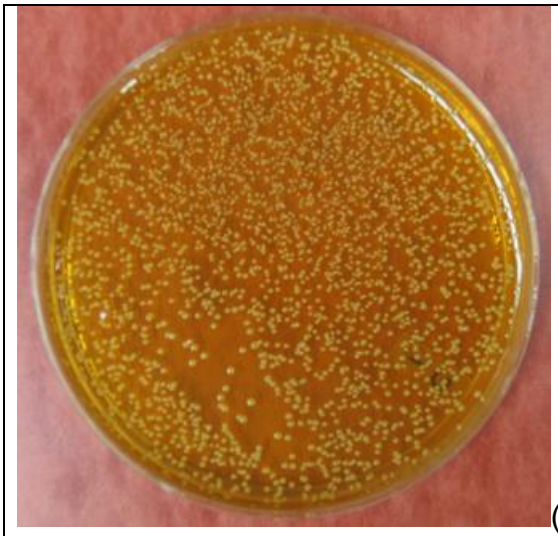
(A)


(B)

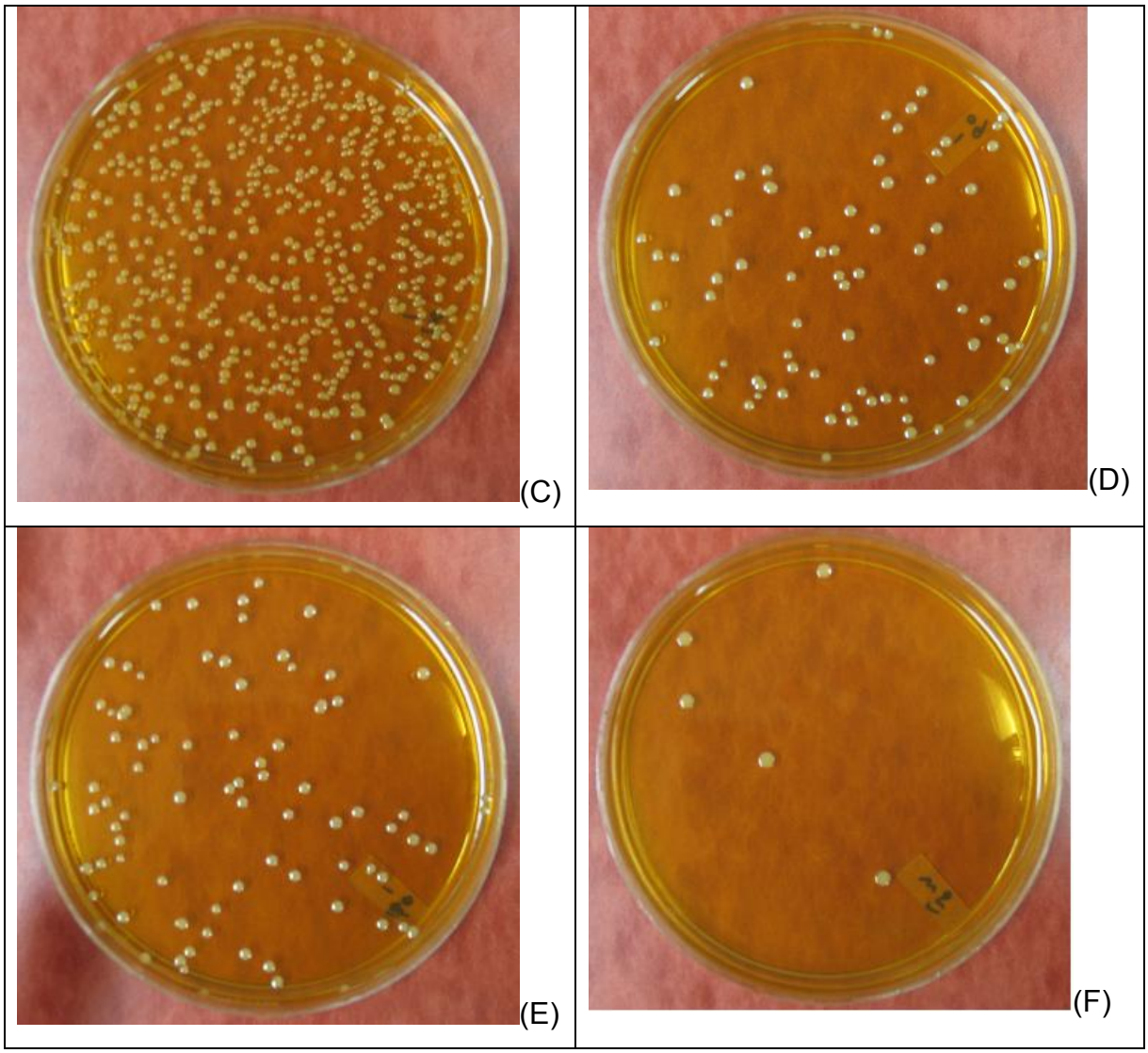

Figure 4.13: Agar plate images of different concentration of *S. aureus*, as well as different concentration of silver nanoparticles. (A) and (B) Control samples, with *S. aureus* concentration of 3000 per agar and 300 per agar, respectively. The bacterial colonies in sample A were too crowding to count, because many of them were actually overlapped due to the limited space. (C) Sample with *E. coli* concentration 3000/agar, and silver concentration of 60 mg/L. Still the colonies were too many to count. (D) Sample with *S. aureus* concentration 300/agar, and silver concentration of 60 mg/L. The number of colonies dropped significantly, compared with the control sample in image (B). (E) Sample with *S. aureus* concentration 3000/agar, and silver concentration of 120 mg/L. As expected, only several colonies were formed. (F) Sample with *S.*

aureus concentration of 300/agar, and silver concentration of 120 mg/L. A few colonies were formed, corresponding to excellent bactericidal property of silver nanoparticles at this concentration.

Table 4.6 listed the number of colonies formed on agar plates for various concentrations of silver nanoparticles. As the numbers on the control sample and the sample of 60-mg/L with 3000/agar bacterial cells were much larger than 300, the measurement of cell colonies is statistically useless as the boundaries between colonies is difficult to distinguished. Therefore, we marked them N/A in the table.

Table 4.6: Numbers of colonies formed on agar plates, overnight.

Concentration of silver nanoparticles	*S. aureus* concentration ~3000/agar	*S. aureus* concentration ~300/agar
0 mg/L (control)	N/A	279 ± 16
60mg/L	N/A	42 ± 14
120mg/L	38 ± 16	< 8

As in the *E. coli* tests, fluorescence images were also obtained for *S. aureus*. The experimental procedures were exactly the same with the previous test. Figure 4.14 depicted these fluorescent microscopic images taken on the *S. aureus* samples.

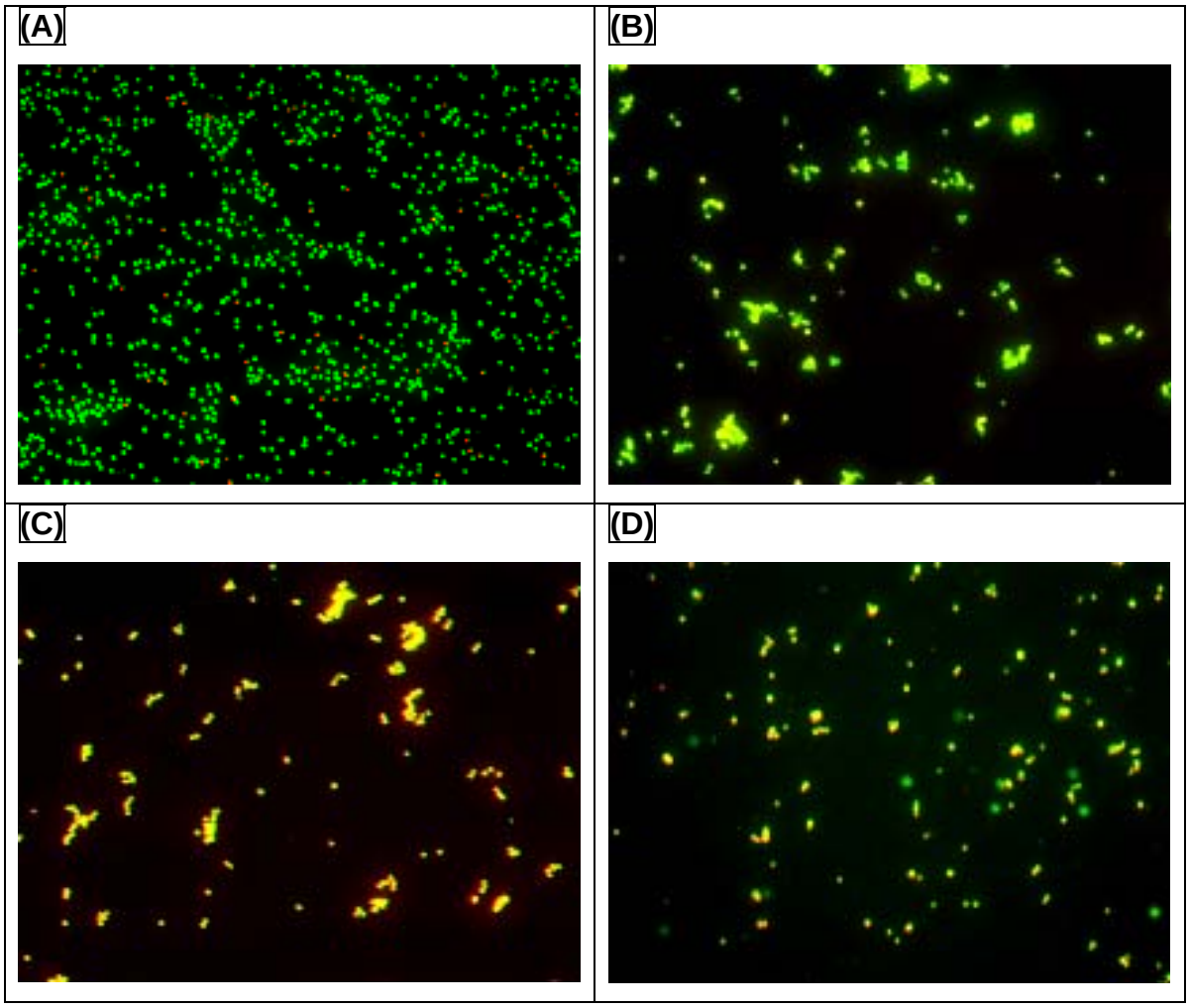

Figure 4.14: Fluorescent microscopic images of *S. aerues* samples with different concentration of silver nanoparticles. (A) Control sample, with no addition of silver nanoparticles. Almost all the cells were green in color. (B) Sample with silver concentration of 30-mg/L. Almost half of the cells fluoresced green. (C) Sample with silver concentration of 60-mg/L. At this silver concentration, some cells were brownish or yellowish. (D) Sample with silver concentration of 120-mg/L. Majority of the bacterial cells were yellowish or brownish.

As illustrated above, image (A) were taken on the control sample, with almost all the cells alive. Image (B), with silver concentration of 30-mg/L, also showed that approximately half of the cells were alive. When the silver concentration was increased to 60-mg/L, some brownish or yellowish cells began

to be observed, depicted in image (C). Therefore, we might consider that the silver nanoparticles started to show their bactericidal effects at this concentration. In addition, at the highest silver concentration, 120-mg/L, most of the cells were yellowish. Corresponding cell numbers were calculated and depicted in **Table 4.7**. And in addition, as we plotted the percentage of dead cells of both *E. coli* and *S. aureus*, they were quite different in number, as depicted in Figure 4.15.

Table 4.7: Number of live and dead cells in different samples, *S. aureus*, showed that most of the bacterial cells been killed as the silver concentration was raised up to 30-mg/L.

	Live	Dead	Live %
0 mg/L (control)	287	<5	~ 100 %
30 mg/L	124	153	45%
60 mg/L	47	268	15%
120 mg/L	24	248	9%

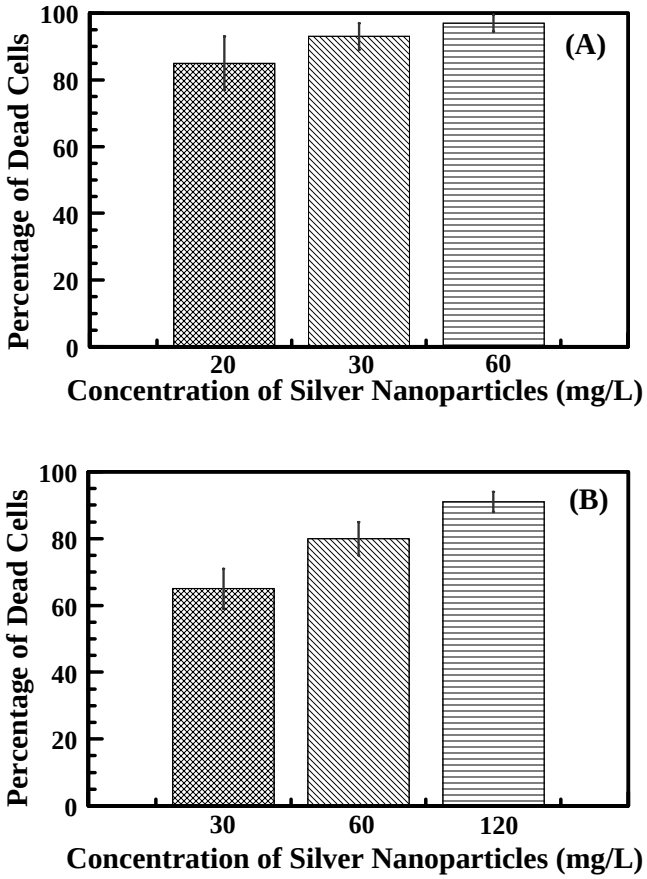

Figure 4.15: Percentage of dead cells versus the concentration of silver nanoparticles. (a) *E. coli*; dead cell percentages were $85 \pm 6\%$, $93 \pm 4\%$, and $97 \pm 2\%$, as the concentration of silver nanoparticles were 20-mg/L, 30-mg/L, and 60-mg/L, respectively. (b) *S. aureus*; dead cell percentages were $65 \pm 6\%$, $80 \pm 5\%$, and $91 \pm 3\%$, as the concentration of silver nanoparticles were 30-mg/L, 60-mg/L, and 120-mg/L, respectively.

CHAPTER 5.
Discussion

5.1. Selection of Reducing Agent

Since the silver nanoparticles used in this project were synthesized via wet chemistry approach, it was crucial to have good control over the particle size as well as its morphology. In general, all chemically based synthesis approaches to metallic nanoparticles start with the reduction of positively charged metal atoms, either as simple ions or as centers of complexes in solution. Solvents can vary from water to very nonpolar media, depending on the nature of the salt or the complex used. The nature of the metal compound also determines the reducing agent to be applied.

As depicted in Figure 5.1, nucleation and growth of metallic nanoparticles in liquid suspension are always considered as four phases. In the first stage of nucleation, the metal salt is reduced to zero-valent metal atoms. These can collide in the solution with metal ions, metal atoms, or clusters to forms an irreversible seed of stable metal nuclei. Depending on the strength of the metal-metal bonds, the difference of the redox potentials between the metal salt, and the reducing agent applied, the diameter of the seed nuclei can be varied, which is typically below 1 nm.

Therefore, the augmentations of the nuclei are due to both their growth in the supersaturated system and to the agglomeration of individual particles, which is also known as coagulation. Thus, a slow rate of formation of new nuclei and rapid aggregation give rise to a small number of large particles, and in contrast, when the rate of formation of the nuclei is high and the growth of aggregates is slow, a colloidal suspension containing a large number of small particles can be obtained. As a consequence, in typical experiments, the selection of proper

reducer(s) is one of the most important issues. Unfortunately, as there is uncertainty in chemistry kinetics, experimental results are always hard to predict. Therefore, the selection and even the concentration of reducer can only be determined empirically.

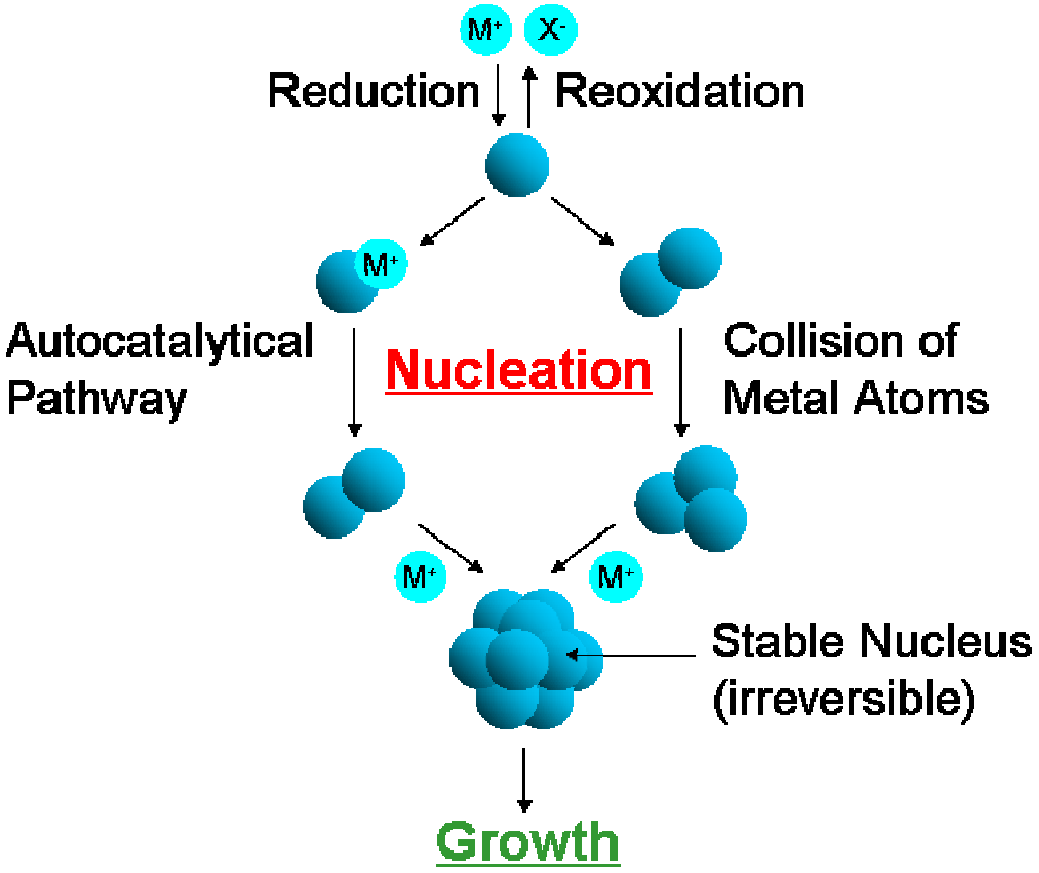

Figure 5.1: General formation procedure of metallic nanoparticles from super-saturated solution. Four phases can be identified, namely ion reduction, collision of metallic atoms, formation of stable nucleus, and the final particle growth stage[62].

Numerous reducing agents are found and characterized by researchers, e.g. sodium citrate, formaldehyde, tannic acid, ascorbic acid, hydrogen, and borohydride. Selection of reducing agents depends on the specific applications. While in synthesis of small, well dispersed metallic nanoparticles, strong reducing agent like hydrogen and borohydride can be applied; in contrast, when relatively

large nanoparticles are required, sodium citrate, formaldehyde are always used, since their reducing ability is low compared with other agents.

In this experiment, formaldehyde and sodium borohydride were examined carefully. After the silica surface activation process with $SnCl_2$ and the addition of silver nitrate solution, either formaldehyde or sodium borohydride was added into the suspension. It was observed that with the addition of formaldehyde, almost one minute was needed for the suspension changing its color from pale yellow to dark yellow; while on the other hand, the suspension's color changed immediately with the addition of sodium borohydride. Although the final suspensions looked identical to each other, as well as the UV-vis absorption spectrums were overlapped perfectly, the differences could be found using transmission electron microscopic (TEM).

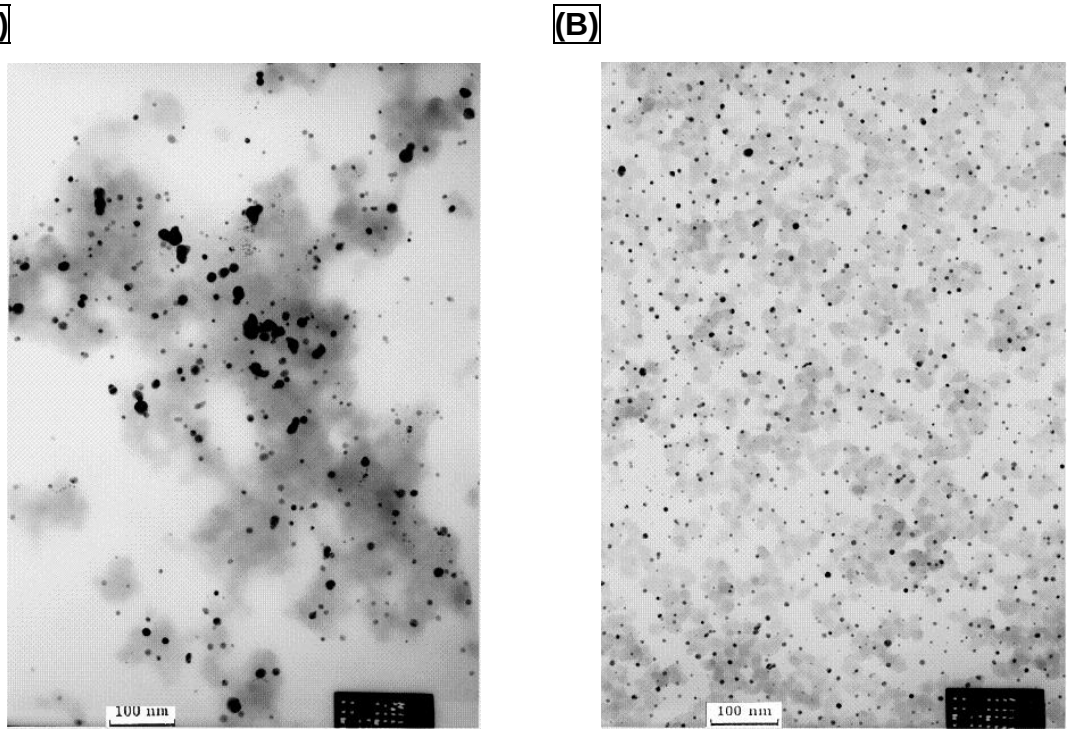

Figure 5.2: Transmission electron microscopic images of silver-silica coupling nanoparticles. (A) Formaldehyde as reducing agent. (B) Sodium borohydride as reducing agent.

As depicted in Figure 5.2, two samples differed in the size of silver nanoparticles, as well as the size distribution. The silver nanoparticles in sample (A), which were reduced by formaldehyde, possessed relatively larger particle size, and in addition, localized clusters could be found all over the image. Whereas for sample (B), which was the sample used during the biological testing performed in this project, sodium borohydride was chosen as the reducer. These silver nanoparticles were considered much more uniform in size and morphology than the particles in sample (A), and also possessed an extraordinary fine dispersion, attached on the silica surfaces. Therefore, we chose sodium borohydride as the reducer in subsequent experiments.

Another important consideration is the concentration of the reducing agent. As discussed earlier, optimum concentration could only be found empirically. For different conditions, such as metallic salt concentration, temperature, and suspension pH, numerous tests should be carried out to determine the concentration of reducer. Moreover, as the heterogeneous nucleation and homogeneous nucleation of metallic nanoparticles can happen at the same time, the determination of reducer concentration becomes even more important to insure that heterogeneous nucleation will dominate.

Two sodium borohydride concentrations were compared, 0.1 M/L and 0.4 M/L. Since 0.1 M/L is a typical concentration used in the synthesis of silver nanoparticles, it was used initially in our experiments. However, the as-synthesized silver nanoparticles tended to be non-uniform in size and morphology (TEM images were not shown here). In particular, particle clusters were easily formed, which made the colloidal suspension unstable over a time scale of several days. This was not completely unexpected as silver concentrations in our experiments were almost 4~6 times higher than the typical concentration researchers used in prior studies. However, we expected that the presence of the silica nanoparticles would help stabilize the silver nanoparticle suspension. The problem was then determined to be the low reducer concentration. In order to maintain the small particle size, more nuclei should be

formed at the beginning; otherwise the growth process would be dominant and then destroy the colloidal stability. Hence, we increased the concentration of sodium borohydride to 0.4 M/L to produce more nuclei and a more stable suspension. This concentration of the reducing agent was used to form the silver nanoparticle suspensions used in ?? experiments.

5.2. Silver-Silica Suspension Stability

The determination of silver-silica nano-composites stability is based on the measurements of the colloids' zeta potential. As described previously, the ionic double layer provides the repulsive force among the surrounding colloids. Both theoretical and practical, zeta potential is highly depend on suspension's pH and can lie anywhere in the range of –100 to +100 mV. However, a dividing line between stable and unstable aqueous dispersions is generally taken at either +30 or -30mV, which means that particles with zeta potentials more positive than +30mV are normally considered stable, as well as the particles with zeta potentials more negative than -30mV. Figure 5.3 shows a typical zeta potential versus suspension pH value for fine silica particles, from which it can be estimated that silica particles are most likely stable in the pH ranges of 2 to 4 and 8 to 12. The isoelectric point, the pH at which the net charge on the silica nanoparticles is zero, is approximately 5.75. Agglomerates are easily formed at this pH.

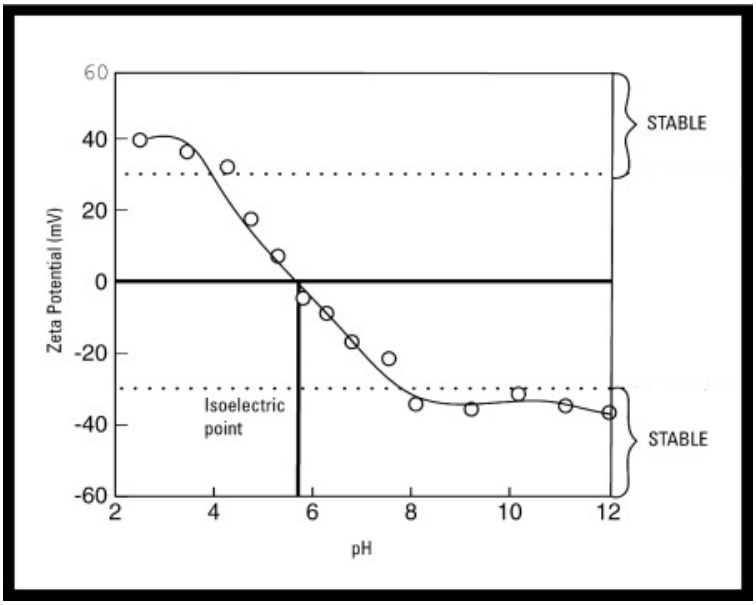

Figure 5.3: Zeta potential versus suspension pH value for fine silica particles. For the pH regions of 2 to 4, and 8 to 12, the absolute particle zeta potential is larger than 30 mV; indicate that the silica particles are considered stable in these pH regions, which is also being confirmed empirically.

Figure 5.4 shows the measured zeta potential of the as-synthesized silver-silica nano-composites. Because of the existence of large amount of silica colloids in the suspension, the overall zeta potential should mainly determined by the silica colloids, which is confirmed by comparing Figure 5.3 and Figure 5.4; the trend lines are following almost the same fashion. The isoelectric points of two curves occur at almost the same pH value, showing that the properties of the silver-silica nanoparticles are dominated by colloidal silica particles' electropotential system.

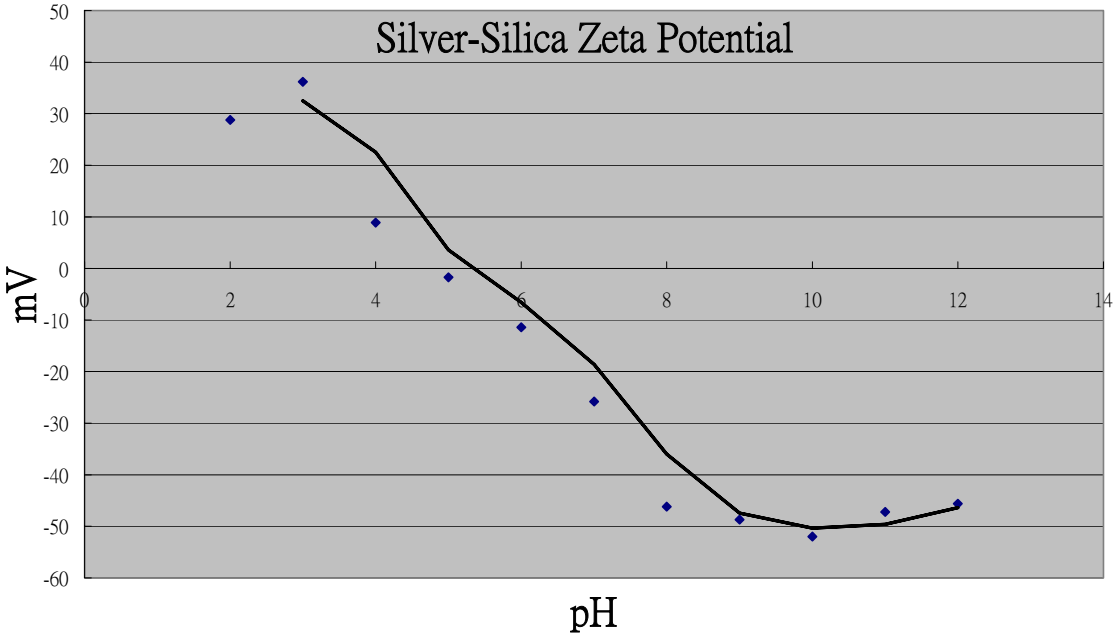

Figure 5.4: Measured zeta potential of the silver-silica nano-composites versus different pH values. Considering -30 mV and +30 mV to be the separators of stable and unstable region, the as synthesized nano-composite is stable when suspension's pH is lower than 3, or higher than ~7.

Based on the measurements of the as-synthesized silver-silica nano-composites' zeta potential, it is clear that most of the absolute values of the zeta potential in our desired pH regions are larger than 30 mV, indicates that the silver-silica suspension can be considered stable upon these pH ranges. Empirically, it is found out that the silver-silica suspension is stable for more than two years when stored in refrigerator, with almost no precipitate observed.

5.3. Anti-Microbial Effects of Nano-Silver Colloids

Bacterial growth curve is one of the key tools microbiologists use to determine the anti-microbial properties of a substance. The growth curve

represents the overall duplicability of the bacterial population. In this project, we generated the growth curves both for *E. coli* and *S. aureus* as a function of the silver nanoparticles concentration. For the convenience of discussion, we re-plot Figure 4.5 and Figure 4.8, and are shown in Figure 5.5 and Figure 5.6:

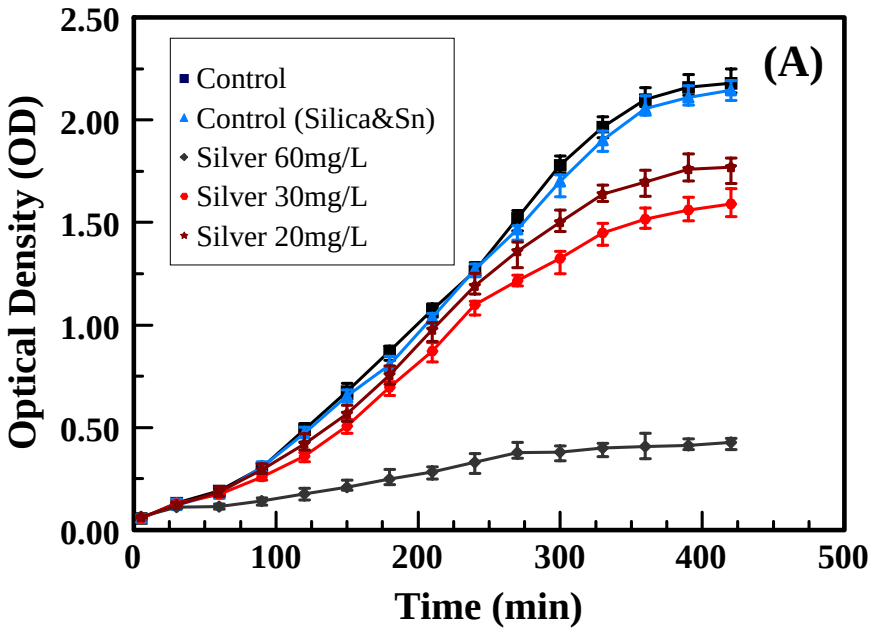

Figure 5.5: Bacterial growth curves of *E. coli* (optical density versus time). As the concentration of silver nanoparticles was increased from 20-mg/L to 60-mg/L, the bacterial optical density decreased significantly.

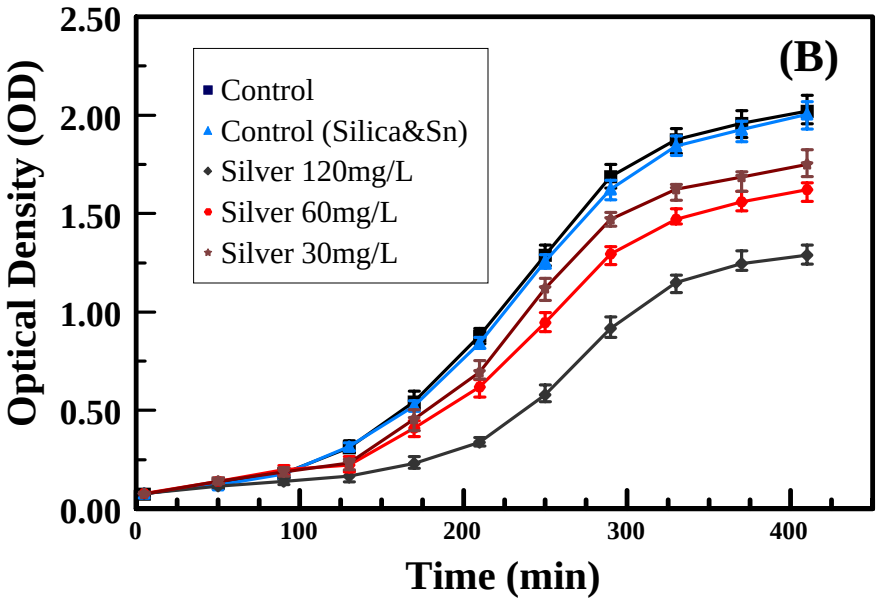

Figure 5.6: Bacterial growth curves of *S. aureus* (optical density versus time). Analogous to *E. coli*, as we increased the silver concentration, the bacterial optical density of *S. aureus* dropped. However it required much higher concentration of silver nanoparticles to make this trend significant.

Low concentrations of silver nanoparticles have strong effects on the growth of *E. coli*. There is no significant population growth when the concentration of the silver nanoparticles reaches 60-mg/L (20 nM). Furthermore, the bacterial viability tests indicates that less than 3 percent of *E. coli* cells are still viable after the treatment of 60-mg/L of silver nanoparticles. Therefore, we conclude that the silver nanoparticles are a strong bactericide to *E. coli*.

When we compare our data with previous research on the bactericidal effects of silver nanoparticles[21,63], the three sets of data do not match perfectly due to the different experimental conditions,. In Sondi's experiments, 40 nM silver nanoparticles can only prohibit the *E. coli* growth to a relatively low level, however most of the bacterial cells are still alive following the nanoparticle treatment. To understand the difference from our results and these other two reports, we have first concluded that their particles to be unstable during the biological test and likely agglomerated and precipitated out of solution during

their studies. As is showed clearly from the SEM images in Ref. 21, nanoparticles were aggregated into clusters. While for our samples, the nanoparticles possessed excellent stability when we utilized the silica colloids as the stabilizers, which is also strongly supported by the measurements of particle zeta potential. The second difference lies in the particle size. Sondi's nanoparticles had the average diameter of about 14 nm[21], while the particles we synthesized are about 5 nm in diameter. The disparity in size causes great difference in particle surface area, which should in return has big impact on the efficiency of the nanoparticles.

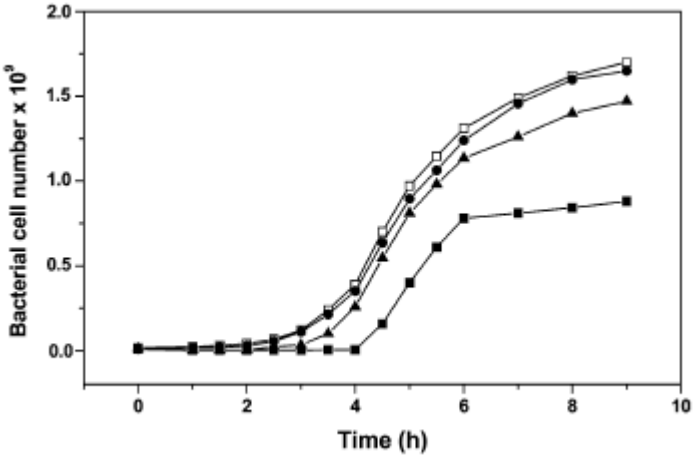

Figure 5.7: Growth curves of *E. coli* in LB medium inoculated with 107 colony forming units (CFUs) of bacteria in the presence of different concentrations of silver nanoparticles[21]: (□) 0, (●) 10, (▲) 50, and (■) 100 μg cm−3.

Lok[63] has done another similar experiment to investigate the anti-microbial properties of silver nanoparticles from bacterial proteome point of view. Some of their findings are:

1. Silver nanoparticle will elicit an immediate and sustained inhibition of *E. coli* cell proliferation;
2. The existence of silver nanoparticles will stimulate the generation and accumulation of cell envelope protein precursors, which inhibits their processing into shorter, mature forms, and finally results in bacterial short lifetime; and

3. Since the envelope protein precursors cannot efficiently form the outer membrane, bacterial cells become more susceptible to the bacteriolytic action of amphiphilic molecules.

Lok's research provided a good explanation why the silver nanoparticles would have anti-microbial properties. However, it requires much higher concentration of silver nanoparticles to show the same bactericidal effects in our sample (22 nM) than Lok's sample (0.8 nM), although the reason is still unknown to us.

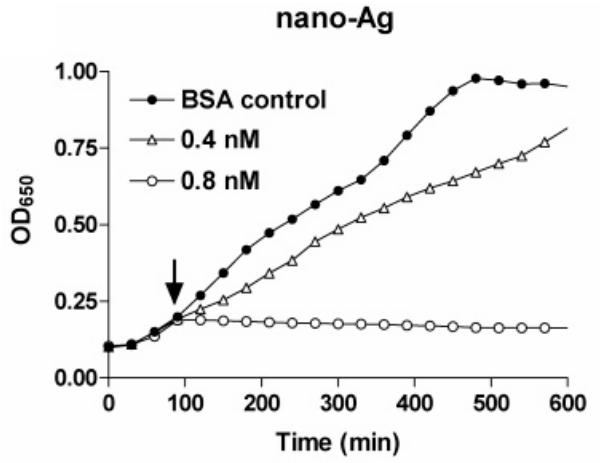

Figure 5.8: Antibacterial activities of nano-Ag. *E. coli* cells were grown at 35 °C to the early exponential phase (O. D.650 = 0.15) in M9 defined medium. Nano-Ag (0.4 and 0.8 nM, stabilized with BSA) was added at the time indicated by the arrows and the O. D.650 was monitored continuously[54].

While most of the previous work is done on *E. coli*, which is a Gram-negative bacterium, little is known about the effects and the mechanisms of silver nanoparticles against Gram-positive bacterium. Compared with E. coli, S. aureus cells' growth is much more difficult to inhibit, and are even harder to be killed, based on the bacterial growth test and viability test results. Unfortunately, we were not able to identify the mechanism associated with either the inhibition of cell growth or cell killing of this Gram-negative bacteria.

CHAPTER 6.

Summary

Silver nanoparticles were synthesized through wet chemistry method, where nanoscale silica particles served as heterogeneous nucleation sites as well as stabilizers. Suspensions were found to be stable at high silver concentrations over a broad pH range, (<3 or >7). By selecting appropriate combinations of reducer and silver concentration, the as-synthesized silver particles are around 5 nm in diameter. Scanning electron microscopy (SEM) and transmission electron microscopy (TEM) were used to reveal the formation and the corresponding morphology of the silver-silica coupling nanoparticles. Ultra-violet visible (UV-vis) scanning spectrophotoscopy was used to detecting the distinct absorption spectrum of silver nanoparticles. The antimicrobial activities of these silver-silica coupling nanoparticles were investigated. *E. coli* and *S. aureus* were used as representatives of Gram-negative and Gram-positive bacteria, respectively. Bacteriological tests showed either bacterial growth inhibition or cell death occurred, depending on the concentrations of silver nanoparticles and the type of bacteria that was testing on. Fluorescent microscopic images were also provided to confirm the bacterial viability after several hours' treatment with silver nanoparticles. Our data showed that large proportions of bacteria were killed upon treatment with silver nanoparticles. In addition, with even low concentrations of silver nanoparticles, bacteria growth inhibition could occur, which also resulted in greatly reducing the amount of live bacteria comparing with the control sample. However, with much more thick and robust cell wall, *S. aureus* possess higher resistance to silver nanoparticles than *E. coli*, which was also observed in many other studies.

References

[1] Henglein, A.; *J. Phys. Chem.,* **1993**, 97(21), 5457-5471.

[2] Mulvaney, P.; *Langmuir*, **1996**, 12(3), 788-800.

[3] U. Kreibig and M. Volmer, Optical Properties of Metal Clusters, Springer Series in Material Science Vol. 25 (Springer-Verlag, Berlin, **1995**).

[4] C. F. Bohren and D. R. Huffman, Absorption and Scattering of Light by Small Particles (John Wiley & Sons Inc., New York, **1998**).

[5] K. Sakoda, Optical Properties of Photonic Crystals, Springer Series in Optical Sciences Vol. 80 (Springer-Verlag, Berlin, **2001**).

[6] S. Nie and S. R. Emory; *Science*, **1997**, 275, 1102-1106.

[7] K. Kneipp et al.; *Phys. Rev. Lett*., **1997**, 78, 1667-1670.

[8] H. Xu, E. J. Bjerneld, M. Ka, and L. Börjesson; *Phys. Rev. Lett*., **1999**, 83, 4357-4360.

[9] D.W. Pohl and D. Courjon, Near Field Optics; NATO ASI, Ser. E, Vol. 241 (Kluwer, Dordrecht, **1993**).

[10] T. Hamouda, M. Hayes, Z. Cao, R. Tonda, K. Johnson, W. Craig, J. Brisker, J. Baker; *J. Infect. Dis*., **1999**, 180, 1939-1949.

[11] P.K. Stoimenov, R.L. Klinger, G.L. Marchin, K.J. Klabunde; *Langmuir*, **2002**, 18, 6679-6686.

[12] Monafo, W.W. and Freedman, B.; *Surg. Clin. North Am*., **1978**, 67, 133-145.

[13] Becker, R.O.; *Met.-based Drugs*, **1999**, 6, 297-300.

[14] Sampath, L.A., Chowdhury, N., Caraos, L. and Modak, S.M.; *J. Hosp. Infect*., **1995**, 30, 201-210.

[15] I. Brigger, C. Dubernet, P. Couvreur, *Adv. Drug Deliver. Rev.* **2002**, 54, 631.

[16] F. Forestier, P. Gerrier, C. Chaumard, A.-M. Quero, P. Couvreur, C. Labarre, *J. Antimicrob. Chemother.* **1992**, 30,173.

[17] L. Joguet, I. Sondi, E. Matijevi´c, *J. Colloid Interface Sci.* **2002**, 251, 284.

[18] M.L. Hans, A.M. Lowman, Curr. *Opin. Solid State Mater.* **2002**, 6, 319.

[19] R.M. Slawson, M.I. Van Dyke, H. Lee, J.T. Trevors, *Plasmid.* **1992**, 27, 72.

[20] G.J. Zhao, S.E. Stevens, *Biometals.* **1998**, 11, 27.

[21] Ivan Sondi, and Branka Salopek-sondi; *J. Colloid Interface Sci*., **2004**, 275, 177-182.

[22] J. Weissmuller, Synthesis and Processing of Nanocrystalline Powder, TMS, Waarendale, PA, **1996**.

[23] G.R. Wiese and T.W. Healy, *Trans. Faraday Soc.* **1970**, 66, 490.

[24] K.T. Miller and c.F. Zukoski, Semiconductor Nanoparticles, Physical, Chemical and Catalytic Aspects, pp. 23-57. (Elsevier, Amsterdam, **1948)**.

[25] J.H. van der Waals, Ph.D Thesis, (University of Leiden, **1873)**.

[26] R.J. Hunter, Foundations of Colloid Science, (Oxford Univ. Press, New York, **1989)**.

[27] J.N. Israelachvili, Intermolecular and Surface Forces, (Academic Press, San Diego, **1992)**.

[28] W.B. Russel, D.A. Saville, and W.R. Schowalter, Colloidal Dispersions, (Cambridge Univ. Press, Cambridge, U.K. **1990)**.

[29] G. Gouy, *J. Phys. Chem.* **1910**, 9, 457.

[30] D.L. Chapman, *Philos. Mag.* **1913**, 25, 475.

[31] O.Z. Stern, *Electrochemistry*, **1924**, 30, 508.

[32] A.N. Patil, D.Y. Paithankar, N. Otsuka and R.P. Andres, *Z. Phys. D* **1993**, 26, 135.

[33] L. M. Liz-Marzan and A. P. Philipse, *J. Phys. Chem.* **1995**, 99, 15120.

[34] W. Stöber, A. Fink and E. Bohn, *J. Colloid Interface Sci.* **1962**, 26, 62.

[35] Liz-Marza´n, L. M.; Philipse, A. P. *J. Colloid Interface Sci.* **1995**, *176*, 459.

[36] Liz-Marza´n, L. M.; Giersig, M.; Mulvaney, P. *J. Chem. Soc.*, *Chem. Commun.* **1996**, 731.

[37] Liz-Marza´n, L. M.; Giersig, M.; Mulvaney, P. *Langmuir* **1996**, *12*, 4329.

[38] P. Mulvaney, M. Giersig, and A. Henglein, *J. Phys. Chem*. **1993**, 97, 7061.

[39] A. Henglein, P. Mulvaney, A. Holzwarth, T.E. Sosebee, and A. Fojtik, Ber. Bunsenges. *Phys. Chem.* **1992**, 96, 754.

[40] P.B. Johnson and W. Christy, *Phys. Rev. B*, **1972**, 6, 4370.

[41] Bruchez M, Moronne M, Gin P, Weiss S, Alivisatos AP: Semiconductor nanocrystals as fluorescent biological labels. *Science* **1998**, 281, 2013.

[42] Chan WCW, Nie SM: Quantum dot bioconjugates for ultrasensitive nonisotopic detection. *Science* **1998**, 281, 2016.

[43] Mah C, Zolotukhin I, Fraites TJ, Dobson J, Batich C, Byrne BJ: Microsphere-mediated delivery of recombinant AAV vectors *i vitro* and *in vivo*. *Mol Therapy* **2000**, 1, S239.

[44] Panatarotto D, Prtidos CD, Hoebeke J, Brown F, Kramer E, Briand JP, Muller S, Prato M, Bianco A: Immunization with peptide-functionalized carbon nanotubes enhances virus-specific neutralizing antibody responses. *Chemistry&Biology* **2003**, 10, 961.

[45] Edelstein RL, Tamanaha CR, Sheehan PE, Miller MM, Baselt DR, Whitman LJ, Colton RJ: The BARC biosensor applied to the detection of biological warfare agents. *Biosensors Bioelectron* **2000**, 14, 805-813.

[46] Nam JM, Thaxton CC, Mirkin CA: Nanoparticles-based bio-bar codes for the ultrasensitive detection of proteins. *Science* **2003**, 301, 1884-1886.

[47] Mahtab R, Rogers JP, Murphy CJ: Protein-sized quantum dot luminescence can distinguish between "straight", "bent", and "kinked" oligonucleotides. *J Am Chem Soc* **1995**, 117, 9099-9100.

[48] Ma J, Wong H, Kong LB, Peng KW: Biomimetic processing of nanocrystallite bioactive apatite coating on titanium. *Nanotechnology* **2003**, 14, 619-623.

[49] Yoshida J, Kobayashi T: Intracellular hyperthermia for cancer using magnetite cationic liposomes. *J Magn Magn Mater* **1999**, 194, 176-184.

[50] Molday RS, MacKenzie D: Immunospecific ferromagnetic iron dextran reagents for the labeling and magnetic separation of cells. *J Immunol Methods* **1982**, 52, 353-367.

[51] Weissleder R, Elizondo G, Wittenburg J, Rabito CA, Bengele HH, Josephson L: Ultrasmall superparamagnetic iron oxide: characterization of a new class of contrast agents for MR imaging. *Radiology* **1990**, 175, 489-493.

[52] P.K. Stoimenov, R.L. Klinger, G.L. Marchin, K.J. Klabunde; *Langmuir*, **2002**, 18, 6679-6686.

[53] Berger TJ, Spadaro JA, Bierman R, Chapin SE, Becker RO.; *Antimicrob Agents Chemother*., **1976**, 10, 856-860.

[54] Golubovich VN, Rabotnova IL.; *Microbiol*., **1974**, 43, 948-950.

[55] Becker, R.O.; *Met.-based Drugs*, **1999**, 6, 297-300.

[56] Sampath, L.A., Chowdhury, N., Caraos, L. and Modak, S.M.; *J. Hosp. Infect*., **1995**, 30, 201-210.

[57] Monafo, W.W. and Freedman, B.; *Surg. Clin. North Am*., **1978**, 67, 133-145.

[58] Sambrook J., Russell DW; *Molecular cloning: a laboratory manual, 3rd edn*. **2001**.

[59] Gardina, P., Conway, C., Kossman, M., and Manson, M.D. *J. Bacteriol*., **1992**, 174, 1528-1536.

[60] B.P. Dey, C.P. Lattuada; *Microbiology Laboratory Guidebook 3rd Edition*, **1998**.

[61] Heard S.M., Griezer F., Barrachlough C.G., and Sanders J.V., *J. Colloid Interface Sci.*, **1983**, 93, 545-555.

[62] M. Maase, PhD Thesis, (Verlag Mainz, Aachen, **1999)**.

[63] C.N. Lok, C.M. Ho, R. Chen, Q.Y. He, W.Y. Yu, H.Z. Sun, P.K. Tam, J.F. Chiu, and C.M. Che, *J. Proteome Res*. **2006**, 5, 916-924.